Universidad de Cantabria

Facultad
de
Ciencias

TURING's THEORY OF MORPHOGENESIS

(TEORÍA MORFOGENÉTICA DE TURING)

Trabajo de Fin de Grado
para acceder al
GRADO EN MATEMÁTICAS

Autor: Daniel Isla Mazón

Director: Luis Alberto Fernández

Junio - 2024

Agradecimientos

Quisiera expresar en primer lugar mi agradecimiento a Luis Alberto. Gracias por tu dedicación, apoyo y paciencia durante la realización de este trabajo. Tu experiencia y consejos han sido esenciales, gracias por tu cercanía y por hacer que todo haya sido más sencillo. No solo has sido un extraordinario tutor, sino también un ejemplo de profesionalidad y valores que siempre tendré presentes. En resumen, gracias por todo lo que me has aportado a lo largo de estos años, no me imagino otro profesor mejor con el que finalizar mis estudios.

Agradezco también a todos y cada uno de los profesores del grado que me han dado clase durante estos cinco años, quienes siempre me han brindado su ayuda con la mejor predisposición, y por los cuales me he desarrollado tanto como persona como matemático. Mención aparte para Cecilia y Rafa. Gracias también por transmitirme vuestros conocimientos con tanta dedicación, lo cual me ha facilitado la realización de este trabajo.

Por supuesto, a mis padres, una parte fundamental de mi vida cuyo apoyo emocional ha sido crucial durante estos años. Gracias por estar siempre ahí; sin vosotros nada de esto habría sido posible, gracias.

Quiero agradecer también a mis amigos, Iker, Celia, Rafa y compañía, con los que he compartido innumerables momentos, tanto de alegrías como de dificultades, durante estos meses. Por último, agradecer también a Pablo todo el apoyo que me ha dado a lo largo de mi carrera, gracias por ser un guía excepcional.

Gracias, en resumen, a todos aquellos que me habeis acompañado a lo largo de esta importante etapa de mi vida.

Abstract

In 1952, Alan M. Turing introduced a theory to explain the formation of spatial biological patterns that can lead to both differentiated tissues and organs as well as the shapes and spots of many living beings (such as the stripes of zebras or tigers, and sea shells, etc.). He suggested the fundamental role played by certain chemicals (morphogens) that react and diffuse through tissues, formulating these interactions as a system of two nonlinear reaction-diffusion partial differential equations.

We will study the general conditions that these types of systems must satisfy for such patterns to emerge, both from a theoretical and computational point of view, using MATLAB for numerical experiments. We will particularly focus on the Schnakenberg system.

Keywords: Morphogenesis, Turing, biological pattern, reaction-diffusion systems, Schnakenberg, computational experiments

Resumen

En 1952, Alan M. Turing introdujo una teoría para explicar la formación de patrones biológicos espaciales que pueden dar lugar tanto a tejidos y órganos diferenciados como explicar las formas y manchas de muchos seres vivos (rayas de las cebras o los tigres, conchas marinas,...). Sugirió para ello el papel fundamental que juegan unas sustancias químicas (morfógenos) que reaccionan y se difunden a través de los tejidos, formulando dichas interacciones como un sistema de dos ecuaciones en derivadas parciales de reacción difusión no lineales.

Estudiaremos las condiciones generales que deben verificar este tipo de sistemas para que puedan aparecer dichos patrones, tanto desde el punto de vista teórico como computacional, utilizando MATLAB para los experimentos numéricos. En particular nos centraremos en el sistema de Schnakenberg.

Palabras clave: Morfogénesis, Turing, patrón biológico, sistemas de reacción-difusión, Schnakenberg, experimentos numéricos.

Contents

1. Introduction

1.1. Motivation. State of Art

Since the origin of civilization, humans have felt an unrelenting curiosity to understand the mysteries of the life around us. In this sense, biology has historically been, and continues to be, one of the branches of science that most interest elicits. The researches and discoveries made over the time, have revealed information that help human kind to understand our place in the universe and our relationship with the world around us. However, there are still countless fundamental questions that have not been resolved. For instance, simple ones such as the origin of the forms or the patterns in nature, as well as its evolution.

If one visualizes the natural world, considering the astonishing diversity of shapes and structures observed in living organisms, one could ask oneself how this diverse forms of life arise, what biological and physical processes underlie their development or how these forms adapt, change and stabilize (despite being subject to numerous sources of noise).If you find these questions difficult to answer, it is because they remain some of the most profound mysteries in science.

In this context, morphogenesis plays a crucial role. It is the part of embryology that characterizes the development of patterns and shapes in nature, hence a fascinating branch of biology, given the great richness and diversity of patterns in different living beings: from small marine organisms to more complex beings such as moths or leopards as we can see in Figures 1 and 2.

Figure 1: Moth (Hyalophora cecropia). It presents patterns both on its wings, as well as on its antennae and in the striping of its body

Figure 2: Leopard (Panthera pardus). It is known by the pattern of spots all over its skin.

The fundamental importance of pattern and form in biology is thus self-evident. Although molecular genetic studies have led to many advances in determining the elements participating in the process, it is not enough to understand the underlying mechanism, and this is where the strengths of mathematical modelling lie. Not only

are models able to analyse experimental results, but also to predict mechanisms by which populations interact, thus suggesting further experiments. In this context, the understanding of these spatial patterns is one of the greatest scientific challenges today as the mechanism of pattern formation is still unknown, and, although several advances have been made in this regard throughout history, bringing us closer to an understanding, most of these theories are phenomenological and do not focus on the description of the underlying process.

D'Arcy Thompson (1860-1948) was a disruptive biologist that played an important role in this issue, whose train of thought supposed a change in the kind of approaches to this problem. From his point of view, Darwin's theory of evolution had several defects, in the sense that, for instance, the patterns in this theory arise from natural selection, which help the animal to survive and adapt to the environment. The key point here is that, despite being partially true, it does not explain how natural selection conforms a particular pattern neither its evolution so that the animal can adapt itself to the changes its species undergoes over time. He claims in his book "On Growth and Form" [11], that physical processes, combined with structural constraints, are responsible for the emergence of forms in nature, particularly biological forms and patterns, hence excluding the Darwinian explanation.

At those times, as one might expect, the majority of the scientific community came up against him; however, this supposed a turning point which led more and more researchers to tackle the root cause, among whom as we will see, stood out Alan Turing with his morphogenetic theory.

Another inspiring idea was the one suggested by Waddington in [13], cited in Turing's paper. He proposed the idea of organizer molecules that were produced by specific cells and diffused throughout the organism such that eventually other cells settled in the organism, depending on the concentration of these molecules. This is based on the gradient model of diffusion, a process of transport by which molecules move from areas of higher concentrations to smaller ones. This idea, as well as those outlined in "What is life?" [10], where Schrödinger raised some physical questions related to life, motivated Turing to carry out his own approach [3].

1.2. Turing's idea

Alan Turing, a prominent figure in the history of science, was a pioneering mathematician, logician, and cryptographer. He is primarily known for his "Turing Machine" during World War II, a foundational concept that laid the groundwork for modern computing and forever changed our understanding of computation and artificial intelligence.

He was particularly fascinated by the arrangement of certain structures in plants, such as their leaves (which exhibited remarkable symmetry) and interested in how certain forms and patterns in nature could arise spontaneously [4]. Turing eventually published his paper "The chemical basis of morphogenesis" [12] in Philosophical Transactions B in 1952, which has shown to be a landmark publication and nowadays is a field of research

in its own right.

He stablished, firstly, how spatial chemical patterns can form, and secondly, how to relate these patterns to those observed in nature. He postulated a mechanism for the formation of biological patterns, suggesting that they are the consequence of an observable population (for instance, skin cells) responding to populations that diffuse signals, called morphogens (as they plant the seed for the morphogenesis). Specifically, these morphogens are considered chemical reactants unaffected by their environment that diffuse freely acting directly on cells to produce specific cellular responses which end up in the formation of such patterns. Therefore, as it has been mentioned before, given a chemical pattern, the cells respond to it, in the sense that we eventually have a correlation between the chemical pre-pattern, and the patterns we see in nature. Once the prepattern is established, morphogenesis is a slave process.

This mechanism was based on reaction-diffusion systems for two different concentrations of morphogens. Put briefly, we can consider a compound Φ, which plays the role as the activator. It carries out an autocatalytic reaction in order to generate more of itself, whose velocity depends on the current concentration of Φ. Furthermore, in this description, Φ also activates the production of another compound, Ψ, which indeed inhibits the formation of Φ. Therefore, Turing's theory could be understood as the competition between the activation of Φ and the inhibition of Ψ.

The innovation in Turing's idea from the previous ones, is the inclusion of reaction between molecules. Despite chemical reaction and molecular diffusion are normally known as homogenising processes, if we consider a mechanism involving both together, stationary patterns can arise naturally from the system. Moreover, in this model we have an spontaneous breaking of the initial system's homogeneity, which eventually leads to the emergence of a wide variety of patterns (unlike the gradient model, where spatial symmetry is already broken from the beginning by the presence of privileged reference cells). Nevertheless, different diffusions for the compounds are required, so that this competition is not identical in all the region. Actually, the inhibitor has to diffuse more quickly than the activator; otherwise the reaction would end and we would not have pattern. Therefore, if both substances diffuse differently over the region, their influences might change locally, thus Φ and Ψ could dominate one over the over in different regions.

Turing demonstrated mathematically the existence of such patterns under certain conditions. He actually carried out several simulations (in 1952) for a given morphogen system, obtaining the patterns shown in Figures 3 and 4. It is also worth showing the modern versions of these patterns (Figures 5 and 6) to appreciate how, despite the limitations of his time, Turing's work is astonishing.

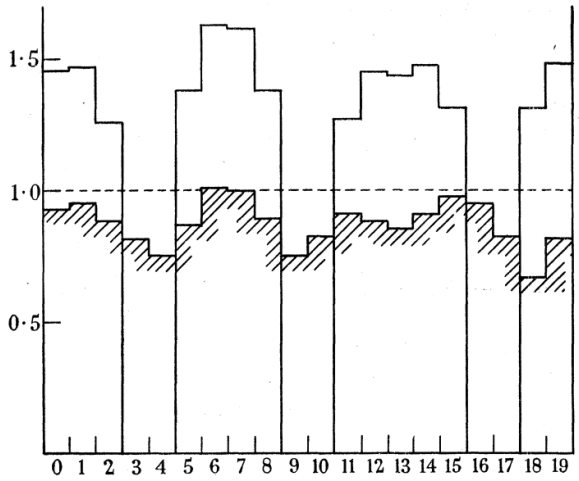

Figure 3: One-dimensional pattern obtained in a numerical simulation published by Turing in 1952

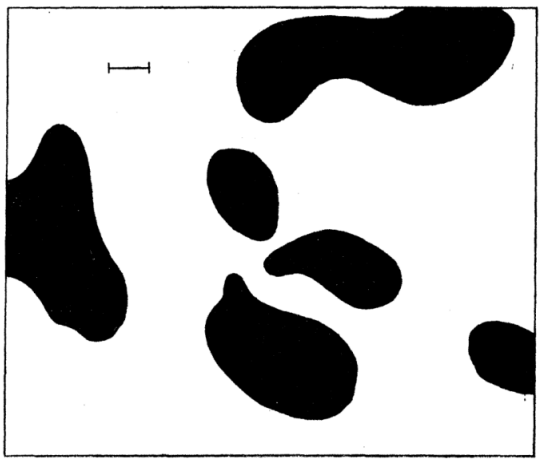

Figure 4: Two-dimensional pattern obtained in a numerical simulation published by Turing in 1952

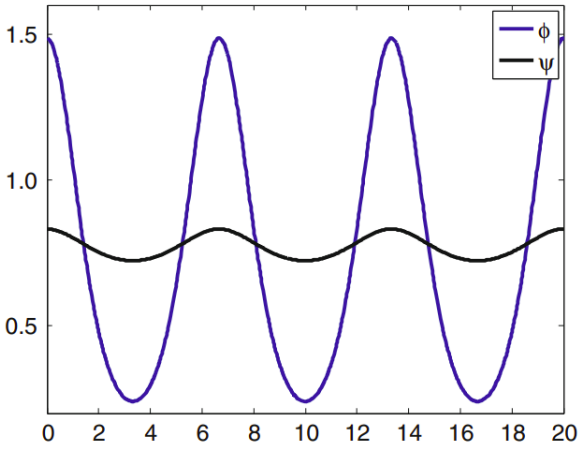

Figure 5: Modern version of the one-dimensional pattern obtained by Turing in 1952

Figure 6: Modern version of the two-dimensional pattern obtained by Turing in 1952

Nevertheless, Turing's ideas were initially neglected by the biological community partly due to the several counterintuitive aspects of the theory. In addition, his work was overshadowed by the discovery of the double-helix structure of DNA a year later, and the subsequent development of molecular biology. His theory had to wait almost 20 years, when chemistry began to pay attention to non-equilibrium processes and physics-mathematics to non-linear problems. Since then, there has been renewed interest in these ideas, and more generally in trying to explain the underlying mechanisms of spatial organisation in developmental biology as well as in the application of Turing's theory to chemical and biological systems. It is worth noting that Turing's original model, and many subsequent papers, have only explored the case of two interacting morphogens, but nowadays it is known that developmental processes involve hundreds of different chemical compounds interacting across a complex and heterogeneous environment.

However, the fundamental insights arising from the concept of diffusion-driven pattern formation are compelling and have been proven in straightforward chemical systems, so it seems likely they play some role in a range of developmental scenarios. Actually,

despite the little knowledge of cellular morphogenesis being known at his time, Turing was prescient in understanding the simplicity of his ideas, stating [12]: "This model will be a simplification and an idealisation, and consequently a falsification. It is to be hoped that the features retained for discussion are those of greatest importance in the present state of knowledge."

Still, his counter-intuitive mechanism, is currently generating new ideas, even after 60 years of research, mainly propelled from the recent rapid developments in computational software and hardware, prompting us to think we could be witnessing the emergence of a new era in Turing theory. For instance, in a recent paper Raspopovic et al. provide evidence to support a Turing mechanism for the arrangement of fingers, by developing a computer model capable of accurately reproducing the patterns that cells follow as the embryo grows fingers [7].

Given the importance of Turing's ideas, we are going to study his theory, analysing the general conditions these systems have to satisfy so that patterns can emerge, both from theoretical and computational point of view. Firstly, we will derive in section 1.3 the form of the reaction diffusion system. Afterwards, we will determine the solution of such system in section 2 and derive the conditions for Turing instability in section 3. Then, we will apply the theory of these previous chapters to several examples in section 4. Finally, we will conclude by discussing the results obtained.

1.3. Reaction Diffusion System Deduction

Particles such as cells, bacteria or chemicals move randomly in nature. The concept of diffusion arises when this microscopic irregular movement results in a macroscopic regular motion of a group of particles. However, there are also different processes that affect particles behaviour, such as interactions either between them or with the environment. Thus, instead of specifying a macroscopic behaviour from the knowledge of the individual microscopic behaviour (which is a complex task to do), it is usual to derive a continuum model equation for the global behaviour in terms of a particle density or concentration of particles or chemicals in our case [5].

Therefore, considering diffusion in three spatial dimensions, let S be an arbitrary surface enclosing a volume V. Denoting the concentration of the species as $\phi(x,t)$ and according to the general conservation equation , the rate of change of $\phi(x,t)$ in V is equal to the rate of flow of material across the surface S into V plus the material created in V. This is,

$$\frac{\partial}{\partial t}\int_V \phi(x,t)dv = -\int_S \mathbf{J}\cdot\mathbf{ds} + \int_V f dv \tag{1}$$

where $\mathbf{J}$ is the flux of material and the function f represents the source of material, which could depend on ϕ, x and t. For instance, in the ecological context, the source term could represent the birth–death process whereas ϕ the population density.

It is possible to simplify previous equation by applying the divergence theorem to

the surface integral and, assuming ϕ (**x**,t) is continuous,

$$\int_V [\phi_t + \nabla \cdot \mathbf{J} - f(\phi, x, t)]\, dv = 0 \tag{2}$$

where ϕ_t denotes the partial derivative with respect to t.

Since the volume V is arbitrary, the integrand must be zero in order to satisfy equation (2) for every value of V. Therefore, the corresponding conservation equation for the concentration ϕ ends up to be

$$\phi_t + \nabla \cdot \mathbf{J} = f(\phi, x, t) \tag{3}$$

In addition, we can follow the classical approach to diffusion, known as Fickian diffusion, which establishes that the flux J of a material is proportional to the gradient of the concentration of the material. Thus, in this three spatial dimension case, we can express the flux as

$$\mathbf{J} = -D\nabla\phi \tag{4}$$

where D could be a function of x and ∇ denotes the gradient with respect to the spatial variables x.

Therefore, equation (3) becomes

$$\phi_t = f(\phi, x, t) + \nabla \cdot (D\nabla\phi) \tag{5}$$

We can generalise the previous expression to the situation in which there are several interacting chemicals represented by the vector $\phi_i(x,t),\ i = 1, ..., m$ of concentrations, each of one diffusing with its own diffusion coefficient, interacting according to the vector source term **f**. Considering this case, equation (5) becomes

$$\boldsymbol{\phi}_t = \mathbf{f} + \nabla \cdot (D\nabla\boldsymbol{\phi}) \tag{6}$$

where D is a matrix of the diffusivities which is a diagonal matrix if there is no cross diffusion among the species. We will mainly be focused on reaction diffusion systems in which D is diagonal and constant and **f** is a function only of $\boldsymbol{\phi}$.

As we have already mentioned before, the main contribution of Turing was the diffusion-driven instability resulting in heterogeneous patterns, which, in some sense, almost seems counter-intuitive as diffusion tends to spread out concentrations, creating homogeneous distributions and not a spatially heterogeneous mixture. It is the interplay of at least two different chemicals which can result in spatial pre-patterns; indeed, we will work with Turing instability at its simplest, studying the interactions between two different diffusing morphogen populations. The typical kinetics that can lead to this instability is the one where one concentration acts as an activator, and the other one, as an inhibitor. The activator promotes its own production, whereas the inhibitor controls the first one in a negative feedback loop [6].

Thus, given two different morphogen concentrations (ϕ, ψ) and taking into account

Neumann boundary conditions (considering an isolated domain as we are interested in self-organisation of pattern i.e without external influence), we have the following system:

$$\begin{cases} \phi_t(x,t) = D_\phi \Delta\phi(x,t) + f\left(\phi(x,t), \psi(x,t)\right) \\ \psi_t(x,t) = D_\psi \Delta\psi(x,t) + g\left(\phi(x,t), \psi(x,t)\right) \\ \nabla\phi(x,t)\cdot\vec{n} = 0, \quad \nabla\psi(x,t)\cdot\vec{n} = 0, \quad x \in \partial\mathbb{D} \\ \phi(x,0) = \phi_0(x), \qquad \psi(x,0) = \psi_0(x) \\ x \in \mathbb{D} \subset \mathbb{R}^{\tilde{d}}, \;\; t > 0 \end{cases} \tag{7}$$

where the functions $f(\phi,\psi)$ y $g(\phi,\psi)$ represent the reaction kinetics (they are, in general, non linear) and $\tilde{d}$ is the space dimension. D_ϕ and D_ψ are the positive constant diffusion coefficients and $\partial\mathbb{D}$ is the boundary of the domain $\mathbb{D}$ where we can define the normal vector $\vec{n}$ at every point.

For instance, in a one spatial dimensional domain $\mathbb{D} = [0, L]$, the reaction diffusion system in equation (7) can be simplified to:

$$\begin{cases} \phi_t(x,t) = D_\phi \frac{\partial^2\phi(x,t)}{\partial x^2} + f\left(\phi(x,t), \psi(x,t)\right) \\ \psi_t(x,t) = D_\psi \frac{\partial^2\psi(x,t)}{\partial x^2} + g\left(\phi(x,t), \psi(x,t)\right) \\ \phi_x(0,t) = \phi_x(L,t) = 0, \;\; \psi_x(0,t) = \psi_x(L,t) = 0 \\ \phi(x,0) = \phi_0(x), \qquad \psi(x,0) = \psi_0(x) \\ x \in [0,L] \subset \mathbb{R}, \;\; t > 0 \end{cases} \tag{8}$$

There is a great variety of reaction models which exhibit Turing pattern formation, although, as we will see and derive, the Schnakenberg model (1979) stands out from the others and is attracting a great deal of research attention in recent years. It is given by the following kinetics:

$$\begin{cases} \phi_t(x,t) = \Delta\phi(x,t) + \gamma\left(a - \phi(x,t) + \phi^2(x,t)\;\psi(x,t)\right) \\ \psi_t(x,t) = d\Delta\psi(x,t) + \gamma\left(b - \phi^2(x,t)\;\psi(x,t)\right) \\ \nabla\phi(x,t)\cdot\vec{n} = 0, \quad \nabla\psi(x,t)\cdot\vec{n} = 0, \quad x \in \partial\mathbb{D} \\ \phi(x,0) = \phi_0(x), \qquad \psi(x,0) = \psi_0(x) \\ x \in \mathbb{D} \subset \mathbb{R}^{\tilde{d}}, \;\; t > 0 \end{cases} \tag{9}$$

This system can be interpreted considering that ϕ and ψ reside in a substrate of two substances A and B. Thus, A can react to produce ϕ and ϕ can degrade to form A again. In this normalised version of the model, these rates correspond to the parameters γa and γ, respectively. In contrast, B reacts to form ψ at rate γb. Also, two molecules of ϕ can react with one molecule of ψ to form three molecules of ϕ at the reaction rate of γ (autocatalysis), which describes the last terms in both expressions of equation. This chemical reaction can be explained with the following equation [1]:

$$\phi \underset{\gamma}{\overset{\gamma a}{\rightleftarrows}} A \quad B \xrightarrow{\gamma b} \psi, \quad 2\phi + \psi \xrightarrow{\gamma} 3\phi \tag{10}$$

In this context, it is often useful and intuitively helpful in model building to express the mechanism's kinetics in schematic terms. We have designed the corresponding scheme of the Schnakenberg model in Figure 7

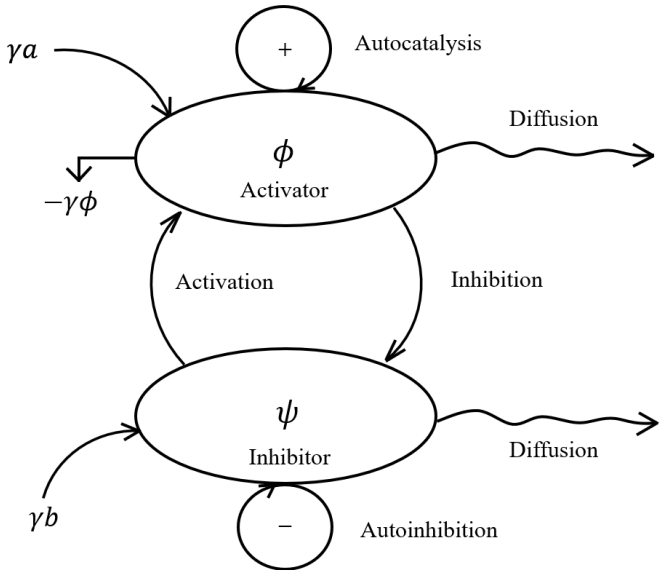

Figure 7: Schematic representation of the activator–inhibitor mechanism in the Schnakenberg system.

2. Solution of the Reaction Diffusion System

2.1. Autonomous System of ODE

Previous equation (8) is a non-linear system of partial differential equations (PDE). However, it is possible to look for constant solutions in x, such that solutions do not depend on the position and, as a result, we get an autonomous system of ordinary differential equation (ODE).

$$\begin{cases} \phi_t(t) = f(\phi(t), \psi(t)) \\ \\ \psi_t(t) = g(\phi(t), \psi(t)) \end{cases} \tag{11}$$

Let us assume there exists $(\phi_0, \psi_0) \in \mathbb{R}^+ \times \mathbb{R}^+$ with $f(\phi_0, \psi_0) = g(\phi_0, \psi_0) = 0$. This represents the case where there is not interaction between the morphogen concentrations. Thus, it is a stationary solution according to (11). Furthermore, since this solution does not depend on space, it is a homogeneous solution, which will remain stationary for the system of PDEs. As previously mentioned, Turing's theory on pattern formation relies on the preexistence of an asymptotically stable solution, making this a fundamental concept.

Let us introduce first the notion of stability.

Definition 1. *The equilibrium solution (ϕ_0, ψ_0) of equation (11) is said to be stable if for each number $\varepsilon > 0$ we can find a number $\delta > 0$ (depending on ε) such that if $(\phi(t), \psi(t))$ is any solution of equation (11) having $||(\phi(0), \psi(0)) - (\phi_0, \psi_0)|| < \delta$, then the solution $(\phi(t), \psi(t))$ exists for all $t \geq 0$ and $||(\phi(t), \psi(t)) - (\phi_0, \psi_0)|| < \varepsilon$ for $t \geq 0$.*

With this in mind, we can define an asymptotically stable solution:

Definition 2. *The equilibrium solution (ϕ_0, ψ_0) is said to be asymptotically stable if it is stable and if there exists a number $\delta_0 > 0$ such that if $(\phi(t), \psi(t))$ is any solution of equation (11) having $||(\phi(0), \psi(0)) - (\phi_0, \psi_0)|| < \delta_0$, then $\lim_{t \to +\infty}(\phi(t), \psi(t)) = (\phi_0, \psi_0)$.*

It is possible to study the stability performing a linear stability analysis, linearizing equation (11) around (ϕ_0, ψ_0) by means of Taylor's formula, neglecting small terms:

$$\begin{aligned} \phi_t = f(\phi, \psi) = f(\phi_0, \psi_0) + f_\phi(\phi_0, \psi_0)(\phi - \phi_0) + f_\psi(\phi_0, \psi_0)(\psi - \psi_0) + ... \\ \psi_t = g(\phi, \psi) = g(\phi_0, \psi_0) + g_\phi(\phi_0, \psi_0)(\phi - \phi_0) + g_\psi(\phi_0, \psi_0)(\psi - \psi_0) + ... \end{aligned} \tag{12}$$

where f_ϕ denotes the partial derivative of f with respect to ϕ and so on.

Taking this into account, we can express approximately the equation (11) as follows:

$$\begin{pmatrix} \phi_t(t) \\ \\ \psi_t(t) \end{pmatrix} \approx \begin{pmatrix} f_\phi(\phi_0, \psi_0) & f_\psi(\phi_0, \psi_0) \\ \\ g_\phi(\phi_0, \psi_0) & g_\psi(\phi_0, \psi_0) \end{pmatrix} \begin{pmatrix} \phi(t) - \phi_0 \\ \\ \psi(t) - \psi_0 \end{pmatrix} \tag{13}$$

Let us note that we now have a homogeneous linear system of ODEs with constant coefficients. To simplify the analysis, we seek exponential solutions, even though the equations are coupled through the matrix shown above.

To proceed, we introduce the vector notation:

$$\mathbf{w} = \begin{pmatrix} \phi - \phi_0 \\ \psi - \psi_0 \end{pmatrix}$$

We know there exist solutions of the form:

$$\mathbf{w} = e^{\lambda t}\mathbf{v}$$

where λ is the eigenvalue of the matrix and $\mathbf{v}$ is the corresponding eigenvector. In this way, we transform the problem into finding the eigenvalues and eigenvectors of the matrix M:

$$M = \begin{pmatrix} f_\phi(\phi_0, \psi_0) & f_\psi(\phi_0, \psi_0) \\ g_\phi(\phi_0, \psi_0) & g_\psi(\phi_0, \psi_0) \end{pmatrix} \tag{14}$$

By solving the characteristic equation of this matrix, we obtain the eigenvalues λ, which indeed determine the stability of the stationary solution (ϕ_0, ψ_0). If the real parts of all eigenvalues are negative, the solution is asymptotically stable; if any of them is positive, it is unstable, whereas if all of them have real part equal to zero, it is stable (although not asymptotically stable). This analysis provides insight into the behavior of the system near the stationary point and helps predict whether small perturbations will grow or decay over time.

Given the role the constant solution of equation (11) has in Turing instability, it is important to ensure that it is an asymptotically stable solution of the ODE.

Theorem 1. The critical point $(0, 0)$ of a linear system $\begin{pmatrix} \phi \\ \psi \end{pmatrix}' = M \begin{pmatrix} \phi \\ \psi \end{pmatrix}$ is asymptotically stable if and only if $\mathrm{Tr}(M) < 0$ y $\det(M) > 0$.

Proof. The characteristic equation of M is given by

$$\det(M - \lambda I) = 0,$$

which can also be written as

$$\lambda^2 - \mathrm{Tr}(M)\lambda + \det(M) = 0,$$

Therefore, the roots of the characteristic equation are the eigenvalues λ_1 and λ_2 of M:

$$\lambda_{1,2} = \frac{\mathrm{Tr}(M) \pm \sqrt{\mathrm{Tr}(M)^2 - 4\det(M)}}{2}. \tag{15}$$

For the critical point $(0, 0)$ to be asymptotically stable, the real parts of both eigenvalues λ_1 and λ_2 must be negative, given the solution of the system. As a consequence, since the sum of the eigenvalues is the trace of M

$$\lambda_1 + \lambda_2 = \mathrm{Tr}(M) < 0.$$

Moreover, the product of the eigenvalues is the determinant of M, hence

$$\lambda_1\lambda_2 = \det(M) > 0.$$

so that both eigenvalues have negative real parts.

These conditions together ($\mathrm{Tr}(M) < 0$ and $\det(M) > 0$) ensure that both eigenvalues λ_1 and λ_2 have negative real parts, as visualizing equation (15), we have three possibilities for the discriminant.

- **Case 1:** $\Delta > 0$**:** The roots λ_1 and λ_2 are real and distinct.
  - If $\mathrm{Tr}(M) < 0$ and $\det(M) > 0$, both roots are negative.
- **Case 2:** $\Delta = 0$**:** The roots λ_1 and λ_2 are real and equal.
  - If $\mathrm{Tr}(M) < 0$, the only repeated root is negative.
- **Case 3:** $\Delta < 0$**:** The roots λ_1 and λ_2 are complex conjugates.
  - The real part of the complex conjugate roots is $\frac{\mathrm{Tr}(M)}{2}$. If $\mathrm{Tr}(M) < 0$, the real part of both roots is negative.

Hence, we have proven that (0,0) is asymptotically stable if and only if $\mathrm{Tr}(M) < 0$ and $\det(M) > 0$.

□

It should be noted that the discussion carried out in the proof, related to the eigenvalues, also applies to the type of solutions we might encounter. The nature of the eigenvalues significantly influences the form and behavior of equation (11) solutions. In the second case of the proof, where the eigenvalues are real and equal, the solution includes linear terms whereas when they are complex conjugates, the solution includes oscillatory terms. Furthermore, the second case has two solution variants depending on if the matrix is diagonalizable or not. Nevertheless, as we will see later, we are going to focus on the case with real and distinct eigenvalues since this will be the most frequent case in our framework.

Stability of an stationary solution is commonly analyzed using phase diagrams. We show in Figure 8 the corresponding trajectory for the case of the autonomous system associated to the Schnakenberg model shown in equation (9), where the constant solution is $\phi_0 = a + b$ and $\psi_0 = b/(a + b)^2$. We can see the asymptotic stability of the stationary solution given a random initial condition point, hence the trajectory converges to the critical point when time goes to infinity.

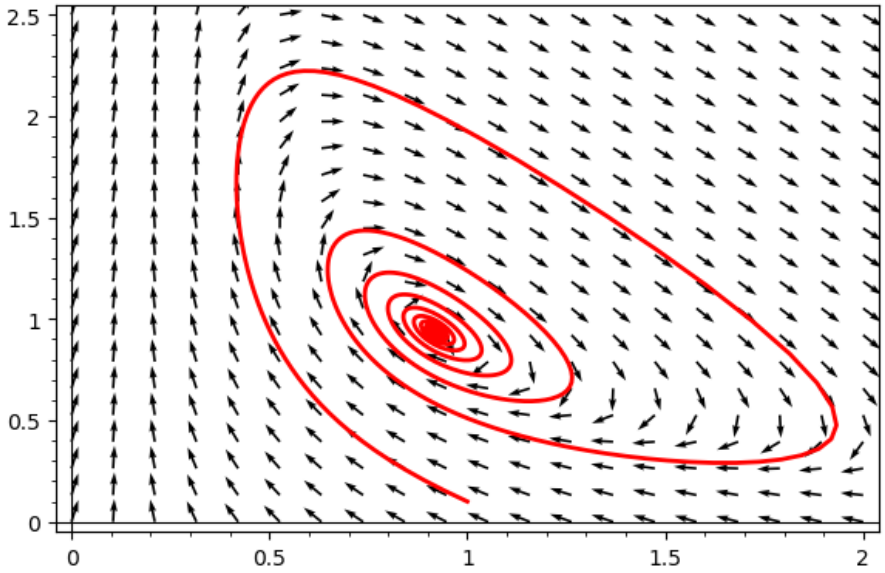

Figure 8: Phase diagram of the Schnakenberg system, for $a = 0.126779$, $b = 0792366$ and $\gamma = 60$.

2.2. General Linear System of PDE

In this first step, we are going to derive the solution of the general linear reaction diffusion system,

$$\begin{cases} \begin{pmatrix} \phi_t(x,t) \\ \psi_t(x,t) \end{pmatrix} = \begin{pmatrix} a_{11} & a_{12} \\ a_{21} & a_{22} \end{pmatrix} \begin{pmatrix} \phi(x,t) \\ \psi(x,t) \end{pmatrix} + \begin{pmatrix} D_\phi & 0 \\ 0 & D_\psi \end{pmatrix} \begin{pmatrix} \Delta\phi(x,t) \\ \Delta\psi(x,t) \end{pmatrix} \\ \nabla\phi(x,t) \cdot \vec{n} = 0, \quad \nabla\psi(x,t) \cdot \vec{n} = 0, \quad x \in \partial\mathbb{D} \\ \phi(x,0) = \phi_0(x), \qquad \psi(x,0) = \psi_0(x) \\ x \in \mathbb{D} \subset \mathbb{R}^{\tilde{d}}, \ \ t > 0 \end{cases} \tag{16}$$

and analyse it for all the spatial dimensions.

It should be noted that we will refer to concentrations and solutions interchangeably by abuse of language although they can be negative as we will actually see later. From now on, we will denote the matrix associated with the concentration term as M:

$$M = \begin{pmatrix} a_{11} & a_{12} \\ a_{21} & a_{22} \end{pmatrix}$$

2.2.1 Spatial dimension one

Considering a one-dimensional domain $\mathbb{D} = [0, L]$, we can use the method of separation of variables and taking into account the boundary conditions, we can try solutions of the form:

$$\phi(x,t) = \sum_{n=0}^{\infty} p_n(t) \cos\left(\frac{n\pi}{L}x\right) \qquad \psi(x,t) = \sum_{n=0}^{\infty} q_n(t) \cos\left(\frac{n\pi}{L}x\right) \tag{17}$$

as they satisfy Neumann conditions since,

$$\frac{\partial \phi(x,t)}{\partial x} = -\sum_{n=0}^{\infty} p_n(t) \frac{n\pi}{L} \sin\left(\frac{n\pi}{L}x\right)$$

and thus we have that $\frac{\partial \phi(0,t)}{\partial x} = \frac{\partial \phi(L,t)}{\partial x} = 0$ where $x \in [0, L]$.

Formally, if we substitute equations (17) into equation (16), we get that:

$$\begin{aligned}\sum_{n=0}^{\infty} \begin{pmatrix} p_m'(t) \\ q_m'(t) \end{pmatrix} \cos\left(\frac{n\pi}{L}x\right) = &\sum_{n=0}^{\infty} \begin{pmatrix} D_\phi & 0 \\ 0 & D_\psi \end{pmatrix} \begin{pmatrix} -\left(\frac{n\pi}{L}\right)^2 p_n(t) \\ -\left(\frac{n\pi}{L}\right)^2 q_n(t) \end{pmatrix} \cos\left(\frac{n\pi}{L}x\right) + \\ &\sum_{n=0}^{\infty} M \begin{pmatrix} p_n(t) \\ q_n(t) \end{pmatrix} \cos\left(\frac{n\pi}{L}x\right)\end{aligned} \tag{18}$$

Then, moving the right term into the left,

$$\sum_{n=0}^{\infty} \left\{ \begin{pmatrix} p_n'(t) \\ q_n'(t) \end{pmatrix} - \left[-\frac{n^2\pi^2}{L^2} \begin{pmatrix} D_\phi & 0 \\ 0 & D_\psi \end{pmatrix} + M \right] \begin{pmatrix} p_n(t) \\ q_n(t) \end{pmatrix} \right\} \cos\left(\frac{n\pi}{L}x\right) = 0$$

However, since the cosines are an orthogonal basis of $\mathrm{L}^2[0, L]$, we have that every term has to be zero:

$$\begin{pmatrix} p_n'(t) \\ q_n'(t) \end{pmatrix} = \left[-\frac{n^2\pi^2}{L^2} \begin{pmatrix} D_\phi & 0 \\ 0 & D_\psi \end{pmatrix} + M \right] \begin{pmatrix} p_n(t) \\ q_n(t) \end{pmatrix} \qquad \forall n \in \mathbb{N} \tag{19}$$

where we will denote the matrix appearing in equation (19) as M_n. This is an homogeneous linear system of two ODEs, with solution of the form:

$$\begin{pmatrix} p_n(t) \\ q_n(t) \end{pmatrix} = A_n \alpha_n \, e^{\lambda_{1_n} t} \; + \; B_n \beta_n \, e^{\lambda_{2_n} t} \tag{20}$$

assuming that λ_{1_n} and λ_{2_n} are real and distinct eigenvalues of M_n and α_n and β_n are the corresponding eigenvectors. The coefficients A_n and B_m are determined with the initial conditions:

$$\begin{aligned}\begin{pmatrix} \phi(x,0) \\ \psi(x,0) \end{pmatrix} = \begin{pmatrix} \phi_0(x) \\ \psi_0(x) \end{pmatrix} = \sum_{n=0}^{\infty} \begin{pmatrix} p_n(0) \\ q_n(0) \end{pmatrix} \cos\left(\frac{n\pi}{L}x\right) \\ \text{with} \quad \begin{pmatrix} p_n(0) \\ q_n(0) \end{pmatrix} = A_n\alpha_n + B_n\beta_n\end{aligned} \tag{21}$$

where we have expanded the initial data in the corresponding Fourier cosine series.

Thus, considering equations (19) and (21), the solution of this system is given by:

$$\begin{pmatrix} \phi(x,t) \\ \psi(x,t) \end{pmatrix} = \sum_{n=0}^{\infty} \left(A_n \alpha_n e^{\lambda_{1n} t} \; + \; B_n \beta_n e^{\lambda_{2n} t} \right) \; \cos\left(\frac{n\pi}{L}x\right) \tag{22}$$

Revisiting the previous discussion on the different cases we might have regarding the eigenvalues, the solution obtained in equation (22) holds only when the eigenvalues are real and distinct. We have different solutions for the rest of possibilities. However, this case is considerably more likely to take place, specially considering the matrix M_n, in which the diffusivity matrix (with $D_\phi \neq D_\psi$) dominates for high enough values of n (it can be inferred from equation (41) below). In addition, in this case two associated eigenvectors form a basis of $\mathbb{R}^2$. Therefore, we will focus in the case with real, negative and distinct eigenvalues.

Although most of the references do not deal with the convergence in equation (22) (as it is a common belief that in nature they converge), we will give our own proof at least in a particular framework that is close to our main interest, as we will see later.

Proof of convergence in the case of M symmetric and a finite number of positive eigenvalues, for $\mathbb{D} = [0, L]$

Proof. Considering the initial conditions in equation (21) $\phi_0, \psi_0 \in \mathrm{L}^2[0, L]$, we trivially have that $\sum_{n=0}^{\infty} p_n^2(0) < +\infty$, and $\sum_{n=0}^{\infty} q_n^2(0) < +\infty$. In addition, considering this initial condition in equation (22) for a fixed value of n, we get that

$$A_n\,\alpha_n \,+\, B_n\,\beta_n = \begin{pmatrix} p_n(0) \\ q_n(0) \end{pmatrix} \tag{23}$$

We aim to prove the convergence of the solution, which is equivalent to see that $\phi(x,t), \psi(x,t) \in \mathrm{L}^2[0, L],\ \forall\, t > 0$. Therefore, from equation (22) we want to show:

$$\begin{aligned} &\sum_{n=0}^{\infty} A_n^2 ||\alpha_n||^2\, e^{2\lambda_{1n} t} < +\infty \\ &\sum_{n=0}^{\infty} B_n^2 ||\beta_n||^2\, e^{2\lambda_{2n} t} < +\infty \end{aligned} \tag{24}$$

We can simplify the previous equation as we have freedom to choose the eigenvectors such that $||\alpha_n|| = ||\beta_n|| = 1$.

In addition, assuming the matrix M to be symmetric, we have that M_n is also symmetric as it is only a modification of the diagonal of M. Therefore, the eigenvectors α_n and β_n of M_n corresponding to the real eigenvalues λ_{1n} and λ_{2n} (which are already normalised) are orthogonal.

Thus, we can express equation (23) as a system:

$$\begin{pmatrix} \alpha_n & \beta_n \end{pmatrix} \begin{pmatrix} A_n \\ B_n \end{pmatrix} = \begin{pmatrix} p_n(0) \\ q_n(0) \end{pmatrix} \tag{25}$$

Then, multiplying both sides by the transpose:

$$\begin{pmatrix} A_n & B_n \end{pmatrix} \begin{pmatrix} \alpha_n & \beta_n \end{pmatrix}^T \begin{pmatrix} \alpha_n & \beta_n \end{pmatrix} \begin{pmatrix} A_n \\ B_n \end{pmatrix} = \begin{pmatrix} p_n(0) & q_n(0) \end{pmatrix} \begin{pmatrix} p_n(0) \\ q_n(0) \end{pmatrix} \tag{26}$$

Since the eigenvectors are orthonormal, from previous expression we deduce that:

$$A_n^2 + B_n^2 = p_n^2(0) + q_n^2(0) \tag{27}$$

Suppose that there exists a finite set I such that if $n \in I$, $\lambda_{1n} > 0$ or $\lambda_{2n} > 0$. Considering again equation (24), we can split the sum, and use the fact that we can always find a constant C such that $0 < e^{2\lambda_{1n}t} \leq C$ and $0 < e^{2\lambda_{2n}t} \leq C \ \forall n \in I$, with $C > 1$. Consequently:

$$\begin{aligned}\sum_{n=0}^{\infty} \left(A_n\, e^{\lambda_{1n}t} + B_n\, e^{\lambda_{2n}t}\right)^2 &\leq 2\left(\sum_{n=0}^{\infty} A_n^2\, e^{2\lambda_{1n}t} + B_n^2\, e^{2\lambda_{2n}t}\right) \leq \\ &\leq 2\sum_{m\in I}\left(A_n^2 e^{2\lambda_{1n}t} + B_n^2 e^{2\lambda_{2n}t}\right) + 2\sum_{m\notin I}\left(A_n^2 + B_n^2\right) \leq \\ &\leq 2C\left(\sum_{n=0}^{\infty} A_n^2 + B_n^2\right) = 2C\left(\sum_{n=0}^{\infty} p_n^2(0) + q_n^2(0)\right)\end{aligned} \tag{28}$$

where the first inequality comes from the fact that if $n \notin I$, its eigenvalues are negative, hence the exponentials are smaller than one. In the second one, we have taken out C as common factor since $C > 1$, and in the last one we have used equation (27). As those sums in equation (28) converge, the solution also does for this case as we wanted to prove. □

It should be noted that the assumption made in the proof regarding the finite number of positive eigenvalues is a consequence of Turing's conditions (which will be derived later). Therefore, as we are studying pattern formation, this hypothesis does not suppose a restriction in our framework.

Apart from the case where M is symmetric, there is also another one for which the solution trivially converges and it is the one where the sum appearing in the initial condition is finite. As a consequence, the solution also has finite terms in its sum (since the cosines are an orthogonal basis of the Hilbert space $\mathrm{L}^2[0, L]$), hence it converges.

2.2.2 Spatial dimension two

Considering a two-dimensional rectangular domain $\mathbb{D} = [0, L_x] \times [0, L_y]$ and analogously as in the one spatial dimension problem (taking into account the boundary conditions in both dimensions), we can try solutions of the form.

$$\begin{aligned}\phi(x, y, t) &= \sum_{n=0}^{\infty}\sum_{m=0}^{\infty} p_{nm}(t)\cos\left(\frac{n\pi}{L_x}x\right)\cos\left(\frac{m\pi}{L_y}y\right) \\ \psi(x, y, t) &= \sum_{n=0}^{\infty}\sum_{m=0}^{\infty} q_{nm}(t)\cos\left(\frac{n\pi}{L_x}x\right)\cos\left(\frac{m\pi}{L_y}y\right)\end{aligned} \tag{29}$$

where $x \in [0, L_x]$ and $y \in [0, L_y]$.

In the same way, we have a similar system as in equation (19):

$$\begin{pmatrix} p'_{nm}(t) \\ q'_{nm}t) \end{pmatrix} = \left[-\left(\frac{n^2\pi^2}{L_x^2} + \frac{m^2\pi^2}{L_y^2}\right)\begin{pmatrix} D_\phi & 0 \\ 0 & D_\psi \end{pmatrix} + M\right]\begin{pmatrix} p_{nm}(t) \\ q_{nm}(t) \end{pmatrix} \tag{30}$$

as well as for the initial condition, for which we get that

$$\begin{pmatrix}\phi(x,y,0)\\ \psi(x,y,0)\end{pmatrix} = \begin{pmatrix}\phi_0(x,y)\\ \psi_0(x,y)\end{pmatrix} = \sum_{n=0}^{\infty}\sum_{m=0}^{\infty}\begin{pmatrix}p_{nm}(0)\\ q_{nm}(0)\end{pmatrix} \; cos\left(\frac{n\pi}{L_x}x\right)\cos\left(\frac{m\pi}{L_y}y\right) \tag{31}$$

hence the general solution for the two spatial dimensional problem is given by

$$\begin{pmatrix}\phi(x,y,t)\\ \psi(x,y,t)\end{pmatrix} = \sum_{n=0}^{\infty}\sum_{m=0}^{\infty}\left(A_{nm}\alpha_{nm}\, e^{\lambda_{1_{nm}}t} \; + \; B_{nm}\beta_{nm}\, e^{\lambda_{2_{nm}}t}\right)\cos\left(\frac{n\pi}{L_x}x\right)\cos\left(\frac{m\pi}{L_y}y\right) \tag{32}$$

where $\lambda_{1_{nm}}$ and $\lambda_{2_{nm}}$ are eigenvalues of M_{nm}, α_{nm} and β_{nm} the corresponding eigenvectors, and A_{nm} and B_{nm} are determined with the initial conditions.

2.2.3 Spatial dimension three

Considering a three-dimensional domain given by the orthohedron $\mathbb{D} = [0, L_x] \times [0, L_y] \times [0, L_z]$, we can carry out the same procedure as in previous two cases, with the difference that now the matrix M_{nmk} is given by:

$$M_{nmk} = \left[-\left(\frac{n^2\pi^2}{L_x^2} + \frac{m^2\pi^2}{L_y^2} + \frac{k^2\pi^2}{L_z^2}\right)\begin{pmatrix}D_\phi & 0\\ 0 & D_\psi\end{pmatrix} + M\right] \tag{33}$$

hence the solution for the three spatial dimensional problem in the orthohedron is

$$\begin{pmatrix}\phi(x,y,z,t)\\ \psi(x,y,z,t)\end{pmatrix} = \\ \sum_{nmk}^{\infty}\left(A_{nmk}\alpha_{nmk}e^{\lambda_{1_{nmk}}t} + B_{nmk}\beta_{nmk}e^{\lambda_{2_{nmk}}t}\right)\cos\left(\frac{n\pi}{L_x}x\right)\cos\left(\frac{m\pi}{L_y}y\right)\cos\left(\frac{k\pi}{L_z}z\right) \tag{34}$$

where $\lambda_{1_{nmk}}$ and $\lambda_{2_{nmk}}$ are eigenvalues of M_{nmk}, α_{nmk} and β_{nmk} the corresponding eigenvectors, and A_{nmk} and B_{nmk} are determined with the initial conditions.

Note that the proof carried out for the convergence in the one-dimensional domain holds for both two and three spatial dimensions.

2.3. General Non-Linear Case

Once we have made the first step and already know the general solution for the linear problem in every dimension at least in simple domains, it is crucial to study the non-linear case, which represents better the processes that take place in nature:

$$\begin{cases} \begin{pmatrix}\phi_t(x,t)\\ \psi_t(x,t)\end{pmatrix} = \begin{pmatrix}f(\phi,\psi)\\ g(\phi,\psi)\end{pmatrix} + \begin{pmatrix}D_\phi & 0\\ 0 & D_\psi\end{pmatrix}\begin{pmatrix}\Delta\phi(x,t)\\ \Delta\psi(x,t)\end{pmatrix} \\ \nabla\phi(x,t)\cdot\vec{n} = 0, \quad \nabla\psi(x,t)\cdot\vec{n} = 0, \quad x \in \partial\mathbb{D} \\ \phi(x,0) = \phi_0(x), \qquad \psi(x,0) = \psi_0(x) \\ x \in \mathbb{D} \subset \mathbb{R}^{\tilde{d}}, \;\; t > 0 \end{cases} \tag{35}$$

The latter actually exhibits a different behaviour from the linear case, which should be noted as the general nonlinear model manifest certain properties (which occur in nature) the linear theory does not predict. While we have formulas for linear theory that provide insights into the behavior of nonlinear cases, concentrations grow unboundedly, and can even be negative. However, for the non linear system, solutions do not grow exponentially (bounded concentrations) and remain positive for positive data (non-negative and bounded) as a consequence of the non-linear terms interaction.

Nevertheless there exist several proofs for different kinetics. For positive and regular enough data, it is possible to prove in particular systems the existence of global bounded solutions. However the proofs are complex and use overly elaborate reasonings that go beyond our scope. For instance, there exist several theorems in [8] which proves it for kinetics which are quite similar to the Schnakenberg case, for spatial dimensions 1,2 and 3.

It corresponds to the Brusselator model appearing in chemical reactions, where the non linear terms are given by:

$$\begin{aligned} f(\phi,\psi) &= a-(b+1)\phi+\phi^2\psi \\ g(\phi,\psi) &= b\phi-\phi^2\psi. \end{aligned} \tag{36}$$

which can be compared with the Schnakenberg functions prior to non-dimensionalization:

$$\begin{aligned} f(\phi,\psi) &= a-\phi+\phi^2\psi \\ g(\phi,\psi) &= b-\phi^2\psi. \end{aligned}$$

In this way, [8] proves the existence of globally bounded solutions for equation (36) and space dimension $\tilde{d}=1,2,3$.

It is also proven for the Gierer-Meinhardt model, proposed in the study of various topics for developmental biology, for which the kinetics are given by:

$$\begin{aligned} f(\phi,\psi) &= \phi^2/\psi+\rho-\mu\phi \\ g(\phi,\psi) &= \phi^2+\overline{\rho}-\nu\psi \end{aligned}$$

where $\mu,\nu,\rho,\overline{\rho}$ are positive constants.

In [8] it is also proved for this case the positivity of the solution for $\tilde{d}=1,2,3$.

However, we have not found an specific reference for a proof explaining this behaviour for the Schnakenberg model (which is the one we have focused on), despite it has attracted a lot of attention in the last years.

Thus, we can conclude that both cases present advantages and disadvantages compared to each other. Given the difficulties encountered in dealing with the nonlinear system, we will use the exact solution of the linear system as an approximation for the solution of the non-linear one in simple domains. Therefore, for instance in the one spatial dimensional problem, we would get:

$$\begin{pmatrix}\phi(x,t)-\phi_0\\ \psi(x,t)-\psi_0\end{pmatrix} \approx \sum_{n=0}^{\infty}\left(A_n\alpha_n e^{\lambda_{1n}t}+B_n\beta_n e^{\lambda_{2n}t}\right)\cos\left(\frac{n\pi}{L}x\right) \tag{37}$$

3. Turing Instability

3.1. Necessary conditions for the Diffusion-Driven Instability

Turing instability arises from the reaction diffusion system analysed previously and it takes place when, under certain conditions, the homogeneous steady state is stable to small perturbations in the absence of diffusion but unstable to small spatial perturbations when diffusion is present. Therefore, we are keen on determining which conditions are necessary so that patterns arise as a consequence of diffusion.

For doing so, as we just have mentioned, we will consider the solutions of the linearized system, hoping they will apply to the solutions of the general nonlinear system. However, we will later see that this is not always true.

We are going to obtain such conditions for the one-dimensional case (we will see later they also hold for the other spatial dimensions). For doing so, we are going to study a particular case of (22), considering $B_n = 0$. This is, approximate solutions for non-linear system of the form [9]:

$$\begin{pmatrix} \phi(x,t) \\ \psi(x,t) \end{pmatrix} = \sum_{n=0}^{\infty} \begin{pmatrix} a_n \\ b_n \end{pmatrix} e^{\lambda_n t} \cos\left(\frac{n\pi}{L}x\right) \tag{38}$$

Note that, if $\mathrm{Re}(\lambda_n)$ is negative for all n, the perturbations tend to decay exponentially quickly, whereas if $\mathrm{Re}(\lambda_n)$ is positive for any value of n, then concentrations in equation (38) will grow exponentially quickly and, as a consequence, the homogeneous steady state turns to be linearly unstable.

With all this in mind, replacing expression (38) into the linearization of (35) for one spatial dimension,

$$0 = \begin{pmatrix} \lambda_n + D_\phi k_n^2 - f_\phi(\phi_0,\psi_0) & -f_\psi(\phi_0,\psi_0) \\ -g_\phi(\phi_0,\psi_0) & \lambda_n + D_\psi k_n^2 - g_\psi(\phi_0,\psi_0) \end{pmatrix} \begin{pmatrix} a_n \\ b_n \end{pmatrix} \tag{39}$$

where $k_n = \frac{n\pi}{L}$.

Previous matrix equation has a non-trivial solution, i.e, $\begin{pmatrix} a_n \\ b_n \end{pmatrix} \neq \begin{pmatrix} 0 \\ 0 \end{pmatrix}$ when the determinant is zero. In the sequel, it is usual to write f_ϕ instead of $f_\phi(\phi_0,\psi_0)$ and so on, to lighten the presentation. In this way, the following expression must be satisfied:

$$\lambda_n^2 + \lambda_n\left((D_\phi + D_\psi)\,k_n^2 - f_\phi - g_\psi\right) + D_\phi D_\psi k_n^4 - k_n^2\,(D_\phi g_\psi + D_\psi f_\phi) + f_\phi g_\psi - f_\psi g_\phi = 0 \tag{40}$$

Denoting $h^2(k) = D_\phi D_\psi k_n^4 - k_n^2\,(D_\phi g_\psi + D_\psi f_\phi) + f_\phi g_\psi - f_\psi g_\phi$, we get that

$$\lambda_{n\pm} = \frac{f_\phi + g_\psi - (D_\phi + D_\psi)k_n^2 \;\pm\; \sqrt{(f_\phi + g_\psi - (D_\phi + D_\psi)k_n^2)^2 - 4h(k_n^2)}}{2} \tag{41}$$

Previous equation (41) is known as dispersion relation and, as we will see, it can be very useful, in the sense that it gives information related to which modes will contribute to the pattern (depending on the sign of the corresponding eigenvalues).

According to equation (41) and considering the case where there is no spatial dependence, the stationary solution must be stable. Thus, in the case where there is no diffusion or spatial variations, $D_\phi = D_\psi = k_n = 0$,

$$\lambda_{n\pm} = \frac{f_\phi + g_\psi \pm \sqrt{(f_\phi + g_\psi)^2 - 4h(0)}}{2} \tag{42}$$

As it was mentioned before, for the homogeneous steady state (ϕ_0, ψ_0) to be linearly stable in the absence of any spatial effects, we need the real parts of both eigenvalues to be negative, $\mathrm{Re}(\lambda_{n\pm}) < 0$ since in this case, the perturbation goes to zero when $t \to +\infty$. For this, the two following conditions must be satisfied according to Theorem 1

$$f_\phi + g_\psi < 0 \tag{43}$$

$$h(0) = f_\phi g_\psi - f_\psi g_\phi > 0 \tag{44}$$

Including now diffusion, D_ϕ, D_ψ and k_n are non-zero values. In this case, $\mathrm{Re}(\lambda_{n_+})$ is required to be positive for at least one n, so that the steady state is unstable to spatial disturbances as regarding equation (43), $f_\phi + g_\psi - (D_\phi + D_\psi)k_n^2 < 0$, $\mathrm{Re}(\lambda_{n_-})$ is always negative (considering previous conditions). Therefore, we will have the instability, according to equation (41) when $h(k_n^2) < 0$ (same reasoning as in the previous case). Expanding the whole expression,

$$D_\phi D_\psi k_n^4 - k_n^2 \left(D_\phi g_\psi + D_\psi f_\phi\right) + f_\phi g_\psi - f_\psi g_\phi \ < \ 0 \tag{45}$$

By solving the corresponding equality for k_n^2, we get

$$k_{n\pm}^2 = \frac{D_\phi g_\psi + D_\psi f_\phi \pm \sqrt{\left(D_\phi g_\psi + D_\psi f_\phi\right)^2 - 4D_\phi D_\psi \left(f_\phi g_\psi - f_\psi g_\phi\right)}}{2D_\phi D_\psi} \tag{46}$$

hence we can divide $\mathbb{R}$ in three different regions: $(-\infty, k_{n-}^2)$,(k_{n-}^2, k_{n+}^2) and $(k_{n+}^2, +\infty)$. Since the expression is positive in the first and in the third one (as k_n^4 is the dominant term), it follows that (k_{n-}^2, k_{n+}^2) is the region of interest, where $h(k_n^2)$ is negative (taking into account the equation (45) is biquadratic and convex). Therefore:

$$k_{n-}^2 < k_n^2 < k_{n+}^2 \tag{47}$$

Note that k_{n-}^2 and k_{n+}^2 are real (by its definition). In addition, considering equation (46) we can see that

$$\left(D_\phi g_\psi + D_\psi f_\phi\right)^2 - 4D_\phi D_\psi \left(f_\phi g_\psi - f_\psi g_\phi\right) > 0$$

Moreover, k_{n+}^2 has to be positive, since it is the square of a real value, so according to equation (46),

$$D_\phi g_\psi + D_\psi f_\phi > 0$$

However, as $f_\phi g_\psi - f_\psi g_\phi > 0$ considering equation (44), the previous inequality system can be simplified to

$$D_\phi g_\psi + D_\psi f_\phi > 2\sqrt{D_\phi D_\psi}\sqrt{(f_\phi g_\psi - f_\psi g_\phi)} > 0 \tag{48}$$

Summarizing, the conditions needed for a Turing instability are given by equations (43), (44), (47) and (48). The first two conditions take into account the solution stability with time, such that the spatial patterns do not change in time, whereas the other two guarantee the instability to spatial perturbations. Once we have a given configuration and the space is fixed, the patterns do not change.

The preceding process allows us to generate spatial patterns under various conditions imposed, given two morphogen concentrations, following equation (16) We collect here again these conditions:

$$\begin{aligned} f_\phi + g_\psi < 0 \qquad & \qquad f_\phi g_\psi - f_\psi g_\phi > 0 \\ k_{n-}^2 < k_n^2 < k_{n+}^2 \qquad & \qquad D_\phi g_\psi + D_\psi f_\phi > 2\sqrt{D_\phi D_\psi}\sqrt{(f_\phi g_\psi - f_\psi g_\phi)} > 0 \end{aligned} \tag{49}$$

It should be reminded that partial derivatives of f and g are evaluated at the critical point (ϕ_0, ψ_0).

We have carried out this derivation for the one-dimensional linear problem. It is worth noting that we have the same conditions for two and three spatial dimensions, modifying respectively $k_n^2 + k_m^2$ and $k_n^2 + k_m^2 + k_k^2$ instead of k_n^2 and changing the notation of the eigenvalues to λ_{nm} or λ_{nmk}.

Remark 1. *Considering expression (38) the dominant contributions as t increases are those in which $Re(\lambda_n) > 0$ since, as it has been mentioned before, the other modes tend to zero exponentially. In addition, in a finite domain, the bounded interval given in equation (47) should have discrete values of k_n.*

Hence, we can rewrite equation (38) for large enough values of t as:

$$\begin{pmatrix} \phi(x,t) \\ \psi(x,t) \end{pmatrix} \simeq \sum_{n_-}^{n_+} \begin{pmatrix} a_n \\ b_n \end{pmatrix} e^{\lambda_n t} \cos\left(\frac{n\pi}{L}\, x\right) \tag{50}$$

Note that this sum converges as it has a finite number of elements.

As a matter of fact, it is possible to understand the basis of the activator-inhibitor mechanism in which the Turing instability is based, introduced in section 1, taking into

account the conditions we have just obtained.

According to the equations (43) and (48), we can conclude that the derivatives $f_\phi(\phi_0, \psi_0)$ and $g_\psi(\phi_0, \psi_0)$ must be of opposite sign, since it follows from the first one that both of them have to be either negative or have opposite sign, but the latter discards the second possibility as the diffusion coefficients are positive. In addition, from the second inequality, we can see that $f_\psi(\phi_0, \psi_0)g_\phi(\phi_0, \psi_0) < 0$ in order to compensate the fact that $f_\phi(\phi_0, \psi_0)g_\psi(\phi_0, \psi_0) < 0$. This leave us with four different combinations for the signs corresponding to $f_\psi(\phi_0, \psi_0)$, $g_\phi(\phi_0, \psi_0)$, $f_\psi(\phi_0, \psi_0)$ and $g_\phi(\phi_0, \psi_0)$. Thus, we have two options for the cross-terms, which are either $f_\psi(\phi_0, \psi_0) < 0$ and $g_\phi(\phi_0, \psi_0) > 0$ or $f_\psi(\phi_0, \psi_0) > 0$ and $g_\phi(\phi_0, \psi_0) < 0$.

Without loss of generality, we can consider the case where $f_\phi(\phi_0, \psi_0) > 0$ and $g_\psi(\phi_0, \psi_0) < 0$. Therefore we have two possibilities. In the first one, where $f_\psi(\phi_0, \psi_0) < 0$ and $g_\phi(\phi_0, \psi_0) > 0$, we can see that ϕ is the activator as $g_\phi(\phi_0, \psi_0) > 0$, and is also self-activating ($f_\phi(\phi_0, \psi_0) > 0$). It is important to take into account that, as we are interested in pattern formation, the inhibitor has to diffuse more quickly than the activator. However, ψ is the inhibitor as $f_\psi(\phi_0, \psi_0) < 0$ and is also inhibiting itself ($g_\psi(\phi_0, \psi_0) < 0$). On the contrary, considering the other case, ψ turns to be the activator $f_\psi(\phi_0, \psi_0) > 0$ although it is self-inhibiting. This two different possibilities we have just explained, can be also understood intuitively in the following diagram:

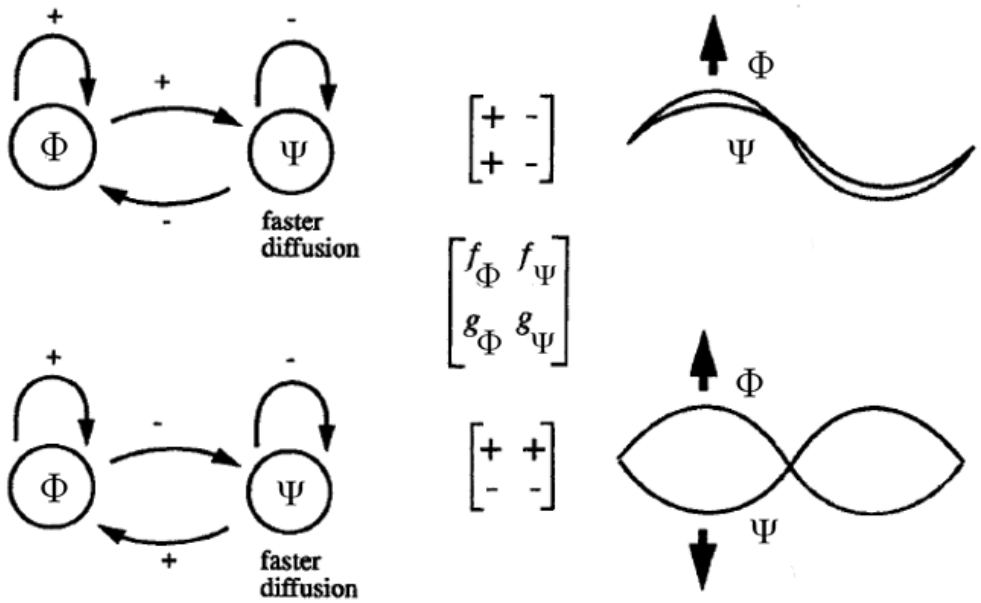

Figure 9: Activator-Inhibitor mechanism for the cases explained

Another difference between both cases is that in the first one, the concentrations follow the same pattern regarding their growths, this is, we have both concentrations either at high or at low densities in the same region as the pattern develops. However, in the second case their behaviour is just the opposite, since where ϕ is at a high density, ψ is low, and vice versa.

3.2. Schnakenberg Reaction-Diffusion System

There is a wide variety of systems that have been used in studies of spatial patterning. Most of them are based on chemical reaction-diffusion system. As it was mentioned previously, Schnakenberg model stands out, which is commonly expressed in the following dimensionless reaction diffusion system:

$$\begin{aligned} \phi_t &= \Delta\phi + \gamma\left(a - \phi + \phi^2 v\right) = \Delta\phi + f(\phi,\psi) \\ \psi_t &= d\Delta\psi + \gamma\left(b - \phi^2\psi\right) \quad = d\Delta\psi + g(\phi,\psi) \end{aligned} \tag{51}$$

with $\gamma > 1$, $d > 1$, $a > 0$ and $b > 0$. In this case, the homogeneous steady state solution turns out to be

$$\phi_0 = a + b, \quad \psi_0 = \frac{b}{(a+b)^2}. \tag{52}$$

as the unique solution to $f(\phi,\psi) = g(\phi,\psi) = 0$.

In addition, we can analyse the conditions derived in equation (49), given that, at the steady state:

$$f_\phi(\phi_0,\psi_0) = \gamma\,\frac{b-a}{a+b}, \quad f_\psi(\phi_0,\psi_0) = \gamma\,(a+b)^2 > 0,$$

$$g_\phi(\phi_0,\psi_0) = \gamma\frac{-2b}{a+b} < 0, \quad g_\psi(\phi_0,\psi_0) = -\gamma\,(a+b)^2 < 0,$$

$$f_\phi(\phi_0,\psi_0)g_\psi(\phi_0,\psi_0) - f_\psi(\phi_0,\psi_0)g_\phi(\phi_0,\psi_0) = \gamma^2\,(a+b)^2 > 0.$$

Therefore, Turing conditions applied to the Schnakenberg model turn out to be:

$$\begin{aligned} f_\phi + g_\psi < 0 &\iff a > \frac{\phi_0}{2}\left(1 - \phi_0^2\right) \\ df_\phi + g_\psi > 2\sqrt{d}\sqrt{f_\phi g_\psi - f_\psi g_\phi} &\iff a < \frac{\phi_0}{2}\left(1 - \frac{2\phi_0}{\sqrt{d}} - \frac{\phi_0^2}{d}\right), \end{aligned} \tag{53}$$

where equation (44) trivially holds and, jointly with $b = \phi - a$, the conditions given in equation (48) are redundant. In addition, equation (47) must be also satisfied in order to have modes with positive eigenvalues.

Therefore, we eventually have two boundary curves in the $(a,b)-$plane which bound the Turing space. As the lower curve does not depend on the diffusion parameter d, it is possible to change the size of the Turing space directly by modifying the value of d, and can even make it disappear. Actually, once Turing's conditions depending on a and b are satisfied, their role turns out to be more like a scaling problem, affecting the concentration values without significantly altering the pattern structure (see [1]). In contrast, γ and d have a more significant impact on pattern shape. The standard requirement that morphogen diffusivities should ideally be considerably different, can be inferred from the equation (53). In this case, the greater the difference in diffusion rates (higher value of d), the wider the Turing space, hence patterns emerge much more easily. Furthermore, γ comes out as a common factor in equation (46) playing a tuning role for the range of modes performing in the solution.

The behaviour mentioned previously can be ilustrated in the following Figures 10, 11, 12 and 13 where, given $a = 0.126779$ and $b = 0.792366$, we can study the dependence of the possible n performing in Turing's instability, with γ and d for the two-dimensional system.

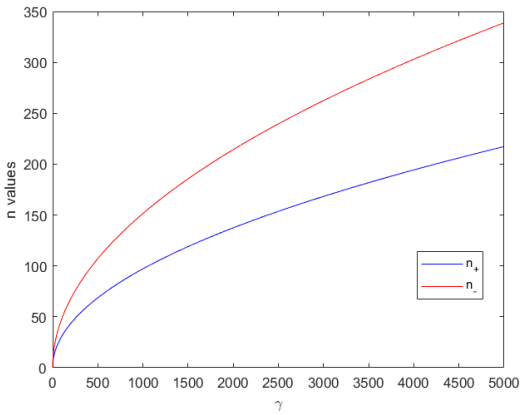

Figure 10: Region with the possible values of n as a function of γ

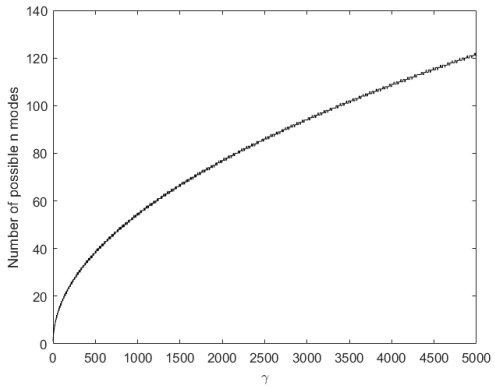

Figure 11: Number of possible n performing in Turing's instability as a function of γ.

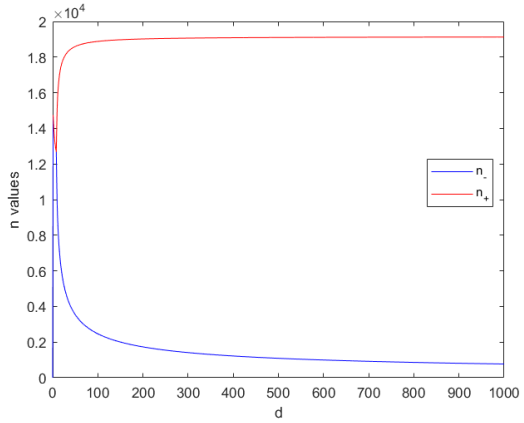

Figure 12: Region with the possible values of n as a function of d

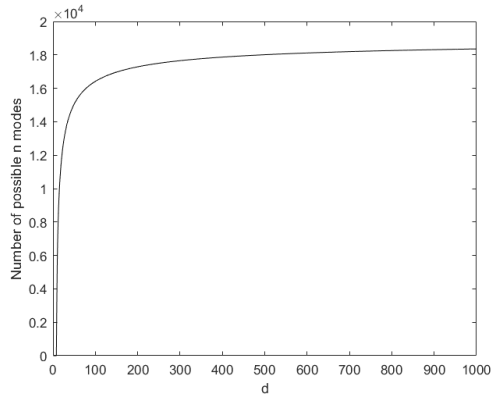

Figure 13: Number of possible n performing in Turing's instability as a function of d

As far as for the dependence with respect to γ is concerned, note that the number of modes with positive eigenvalues grow exponentially initially and then they have a linear correlation. In contrast, despite this range of n also increases exponentially initially with d, it stabilizes asymptotically for a given value of d. This dependence is not particular of this case, but the general behaviour of the solution with these parameters.

It is important to notice that the previous analysis corresponds only to the linear case. Nevertheless, as it has already been mentioned before, there is a huge difference in the non-linear system, arising from the non-linear terms. These non-linear interactions are the responsible of the finite amplitude in the patterns (which indeed makes the model chemically plausible). Moreover, non-linear equations can cause the excitation of higher modes, in the sense that, for instance, quadratic terms give

$$\cos\left(\frac{n\pi}{L}x\right)^2 = \frac{1}{2}\left(1 + \cos\left(\frac{2n\pi}{L}x\right)\right)$$

Thus, higher modes can perform in the solution, and its contribution can be determined from the coefficients of the Fourier expansion in equation (22). Although in the linear approximation concentrations grow unbounded and can even be negative it gives an important hint of what happens in the non-linear case.

4. Numerical Simulations

In this section we are going to analyse and compare different examples for one, two and three dimensions, including both linear and non-linear problems. In particular, we will explore the dependencies of the solution with respect to all the parameters involved.

4.1. MATLAB programs

For our study, we have carried out an extensive numerical experimentation work, by implementing several functions in MATLAB R2023b. Most of them are based on **pdepe** and **solvepde**, tools which solve systems of PDEs specified in a PDEModel. The former, for the one-dimensional domain, uses the ode15s solver for time integration (for solving stiff ODE), whereas the latter, for the two and three spatial dimensions, is based on the finite element method (FEM). We had to provide as input in both programs the domain $\mathbb{D}$, the boundary conditions of the problem, the initial conditions, as well as specify both PDEs. After meshing the domain, the programs solved the problem for different values of time, taking into account the model introduced, to eventually plot the solution and visualize the pattern.

The difficult part of FEM in spatial dimension 2 and 3 is drawing the domain (specially if it is not a simple one) and generating its mesh. Despite MATLAB has his own commands for simple cases, the use of PDE toolboox and STL files (for two and three spatial dimensions, resp.) is required for more complex geometry. Let us recall that STL is a file format widely used for 3D printing. In general, we have used domains with simple geometries (square, cube). As an example, we have included at the end an example with a more complicated 3D geometry (a cat).

We have combined these two programs with the study of the modes whose eigenvalues were positive, once the matrix was defined, so that we could analyse more efficiently the simulations. In addition, we have also created several programs to study the dependence of the solution with respect to the different parameters, plotting the values of n with positive eigenvalues as a function of such parameters. From all these programs, we have carried out all the simulations required for our project. In the appendix we have included a couple of representative examples of the use of both comands.

4.2. Spatial dimension one

4.2.1 Linear Problem

In this section we are going to analyse and compare different cases for the one dimensional linear domain problem. The problem to be addressed is the following:

$$\begin{cases} \begin{pmatrix} \phi_t(x,t) \\ \psi_t(x,t) \end{pmatrix} = M \begin{pmatrix} \phi(x,t) \\ \psi(x,t) \end{pmatrix} + \begin{pmatrix} D_\phi & 0 \\ 0 & D_\psi \end{pmatrix} \begin{pmatrix} \phi_{xx}(x,t) \\ \psi_{xx}(x,t) \end{pmatrix} \\ \phi_x(0,t) = \phi_x(L,t) = 0, \;\; \psi_x(0,t) = \psi_x(L,t) = 0 \\ \phi(x,0) = \phi_0(x), \qquad \psi(x,0) = \psi_0(x) \\ x \in \mathbb{D} = [0,L] \subset \mathbb{R}, \;\; t > 0 \end{cases} \tag{54}$$

In the beginning we are going to consider the matrix

$$M = \begin{pmatrix} 0.5 & 1 \\ -0.55 & -1 \end{pmatrix} \tag{55}$$

with $D_\phi = 1$ and $D_\psi = 10$, for which Turing conditions are satisfied (this can be verified by replacing this values in equation (49)). Indeed, we will keep the value $D_\phi = 1$ in all the examples for simplicity. As for the domain is concerned, we are going to assume $L = 10$.

The only mode with positive eigenvalue for these parameters is $n = 1$. Recalling the notation of equation (22), the eigenvalues for this mode are λ_{11} and λ_{21} where the corresponding eigenvectors are $\alpha_1 = (\alpha_{11}, \alpha_{21})$ and $\beta_1 = (\beta_{11}, \beta_{21})$. This is the notation we will use in what follows.

Without additional preamble, the values obtained in this case are $\lambda_{11} = 1.4309e-01$, $\alpha_1 = (9.6824e-01, -2.5000e-01)$ for the first eigenvalue, and $\lambda_{21} = -1.7287e+00$, $\beta_1 = (-4.2496e-01, 9.0520e-01)$ for the second one. As far as we know, this is the mode that is going to dominate, and thus will get selected by letting time increase.

Once we already have all the parameters fixed, we can study the dependence of the solution with respect to the initial condition. The simplest case is the one where we have constant initial conditions, this is, $(\phi(x,0), \psi(x,0)) = (\hat{\phi}_0, \hat{\psi}_0)$. In this case, we can replace it into equation (22), and we get that

$$\begin{pmatrix} \hat{\phi}_0 \\ \hat{\psi}_0 \end{pmatrix} = A_0 \begin{pmatrix} \alpha_{10} \\ \alpha_{20} \end{pmatrix} + B_0 \begin{pmatrix} \beta_{10} \\ \beta_{20} \end{pmatrix}$$

as the cosines are an orthogonal basis of $\mathrm{L}^2[0,L]$. Since the eigenvectors also form a basis, we can express the initial condition as a linear combination of them.

Furthermore, we can select α_0 as the initial condition:

$$\begin{pmatrix} \hat{\phi}_0 \\ \hat{\psi}_0 \end{pmatrix} = \alpha_0 = \begin{pmatrix} \alpha_{10} \\ \alpha_{20} \end{pmatrix}$$

so that $A_0 = 1$ and $B_0 = 0$, hence the solution is given by

$$\begin{pmatrix} \phi(x,t) \\ \psi(x,t) \end{pmatrix} = \begin{pmatrix} \alpha_{10} \\ \alpha_{20} \end{pmatrix} e^{\lambda_{10}\, t} \tag{56}$$

Eventually, it is possible to study both time and space behaviour of the solution:

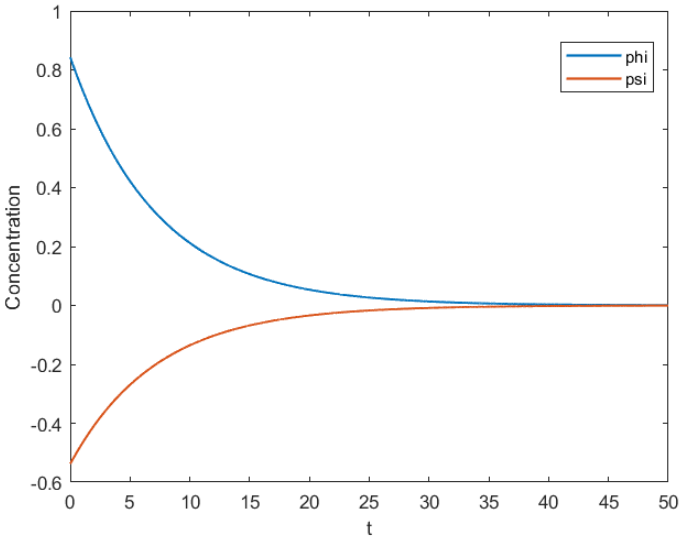

Figure 14: Concentrations over time for system (54) with matrix (55), $D_\psi = 10$ and the constant initial conditions.

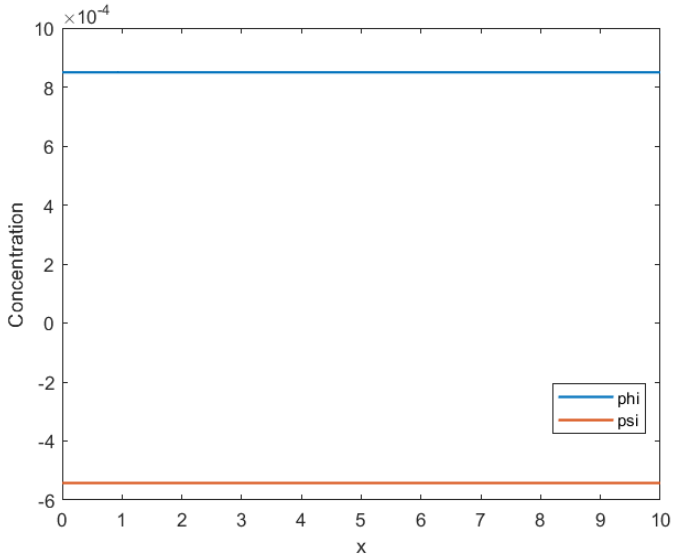

Figure 15: Concentrations over space for system (54) with matrix (55), $t = 50$, $D_\psi = 10$ and the constant initial conditions.

We can see in Figure 14 what we expected theoretically from equation (56). Since the eigenvalue for $n = 0$ is negative ($\lambda_{10} = -1.3819e-01$), the solution tends to zero with time (the constant asymptotically stable solution for the autonomous system) and it does not depend on space, given the initial condition. Thus, if we consider higher values of t, concentrations would be closer to zero.

Note that we have obtained negative concentration values, which has no physical sense. Although this show a clear limitation in linear theory, this approximation is useful to understand how patterns arise, as well as their dependence with the parameters involved in the system.

We can increase the complexity, analysing now non-constant initial conditions; for instance $(\phi(x,0), \psi(x,0)) = (3\cos\left(\frac{2\pi}{10}x\right), -7\cos\left(\frac{2\pi}{10}x\right))$. Analogously as in the previous case, since the cosine form a basis, we can express equation (22) considering only the term corresponding to $n = 2$ (fixed in the initial condition).

$$\begin{pmatrix}\phi(x,t)\\ \psi(x,t)\end{pmatrix} = \left[A_2\begin{pmatrix}\alpha_{12}\\ \alpha_{22}\end{pmatrix}e^{\lambda_{12}t} + B_2\begin{pmatrix}\beta_{12}\\ \beta_{22}\end{pmatrix}e^{\lambda_{22}t}\right]\cos\left(\frac{2\pi}{10}x\right) \tag{57}$$

Furthermore, as it has been explained previously, the coefficients of the initial condition terms can be expressed as a combination of the corresponding eigenvectors, which lead us to determine the values of A_2 and B_2. If we take into account that $\lambda_{12} = -6.0805e{-}03$ and $\lambda_{22} = -4.8365e{+}00$, and also $\alpha_2 = (9.9386e{-}01, -1.1061e{-}01)$, $\beta_2 = (-1.9833e{-}01, 9.8013e{-}01)$, we get that $A_2 = 1.6300e{+}00$ and $B_2 = -6.9579e{+}00$.

The numerical solution can be seen graphically in Figure 16 together with the analytical solution of equation (57) for $t = 100$.

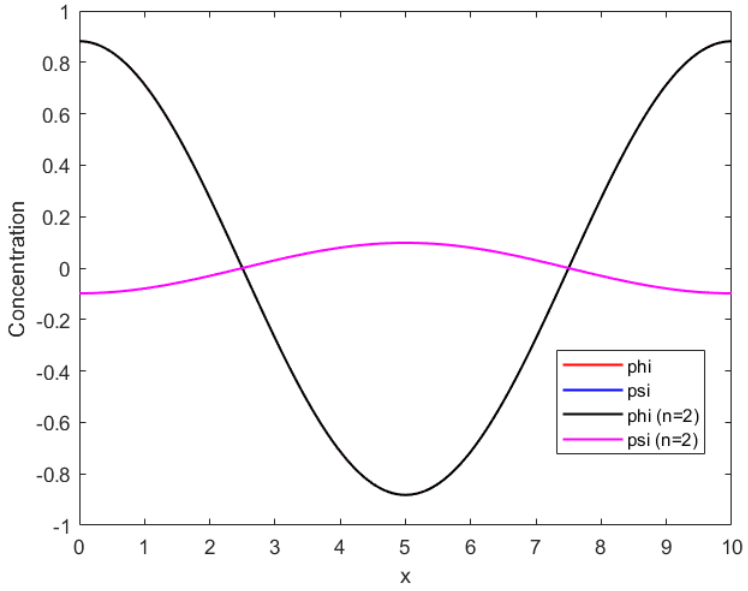

Figure 16: Concentrations over space for system (54) with matrix (55), where $t = 100$, $L = 10$, $D_\psi = 10$ and the initial condition mentioned before, as well as the corresponding analytical solution in equation (22) with $n = 2$.

As far as for the spatial dependence is concerned, we can see in Figure 16 that there are oscillations with an amplitude of 0.8 which actually decrease for higher values of t (since both eigenvalues are negative). We can also observe the cosine behaviour with two nodes performing in equation (57). Furthermore both numerical and analytical solutions for the two concentrations overlap completely. In fact, the maximum relative error for each one is of the order of $\mathrm{O}(10^{-4})$.

It is remarkable that the solution also tends to zero with time as expected, although in a slower way for ϕ than in the previous case since in this case λ_{12} is very close to zero (it is not a too negative value).

Once we have already studied the most straightforward examples, we can try with general initial conditions since every arbitrary function $\phi(x,0), \psi(x,0) \in \mathrm{L}^2[0,L]$ can be expressed in its Fourier series of cosines in the following way

$$\begin{aligned} \phi(x,0) &= \frac{\rho_0}{2} + \sum_{n=1}^{\infty} \rho_m \cos\left(\frac{n\pi}{L}x\right) \qquad \text{where} \qquad \rho_n = \frac{2}{L}\int_0^L \phi(x,0)\cos\left(\frac{n\pi}{L}x\right) \\ \psi(x,0) &= \frac{\delta_0}{2} + \sum_{n=1}^{\infty} \delta_n \cos\left(\frac{n\pi}{L}x\right) \qquad \text{where} \qquad \delta_n = \frac{2}{L}\int_0^L \psi(x,0)\cos\left(\frac{n\pi}{L}x\right) \end{aligned} \tag{58}$$

Furthermore, according to Bessel Inequality, if we have a function which is square-integrable, $\rho_n \longrightarrow 0$ and $\delta_n \longrightarrow 0$ for $n \longrightarrow +\infty$, see [2].

For instance, we can consider an initial condition given by $(\phi(x,0), \psi(x,0)) = (x^2, x^3)$, which does not isolate any value of n in the sum of equation (22). In this case, the solution has now contributions from every value of n although for higher t it will be essentially dominated by the term corresponding to $n = 1$ since it is the only one which has a positive eigenvalue.

We have studied the numerical solution, with the corresponding analytical solution taking into account only the dominant term ($n = 1$) of the sum. When t is small, there are more contributions apart from $n = 1$, hence the analytical solution in which only performs $n = 1$, does not match with the numerical solution. Nevertheless, this changes if we study a high enough value of t (e.g, $t = 100$) for which it is useful to normalise both solutions since they are of the order of $\mathrm{O}(10^6)$. Therefore, we show in Figure 17 the results, dividing both concentrations by their maximum (of the order of $\mathrm{O}(e^{14})$).

In this case, the mode $n = 1$ becomes the main contribution to the solution since t is high enough for the rest to be neglected, hence we can see the cosine behaviour of one node ($n = 1$). We have gained more sensibility with the normalisation, where the absolute errors are of the order of $\mathrm{O}(10^{-7})$ or even smaller. Considering the overlap in Figure 17 between both solutions and the corresponding errors, we can say that they are practically equivalent and the pattern has the expected form.

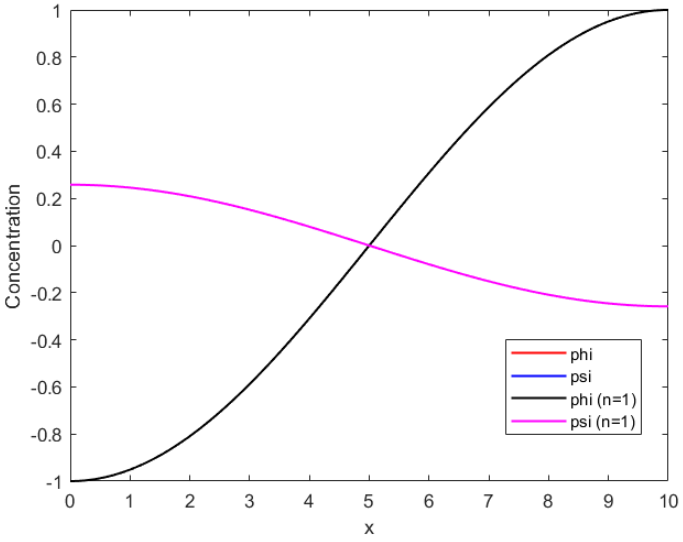

Figure 17: Concentrations normalised over space for system (54) with matrix (55), $t = 100$, $L = 10$, $D_\psi = 10$ and the general initial condition, with its corresponding analytical solution in equation (22) for $n = 1$, also normalised.

Once we have studied the dependence of the solution with respect to the initial condition, we could ask ourselves how it would behave if we change other parameters. Firstly, we are going to see the dependence with respect to the diffusivities, by analysing the previous example, but now with $D_\psi = 100$. In this case, we have positive eigenvalue for $n = 1$ ($\lambda_{11} = 3.5229e-01$, $\lambda_{21} = -1.0820e+01$) and for $n = 2$ ($\lambda_{12} = 9.1659e-02$, $\lambda_{22} = -4.0464e+01$). The corresponding eigenvectors are $\alpha_1 = (9.98806e-01, -4.8952e-02)$, $\beta_1 = (-8.8759e-02, 9.9605e-01)$, $\alpha_2 = (9.99907e-01, -1.3555e-02)$ and $\beta_2 = (-2.4641e-02, 9.9969e-01)$ respectively.

In this case, we have an additional mode that is going to perform in the solution, thus it will be a little more complex as we have two main contributions. However, for high enough values of t, the one whose eigenvalue is the highest, is the one which is going to dominate. Considering only these two terms (neglecting all whose eigenvalues are negative), we can express the analytical solution as:

$$\begin{pmatrix}\phi(x,t)\\ \psi(x,t)\end{pmatrix} \approx A_1 \begin{pmatrix}\alpha_{11}\\ \alpha_{21}\end{pmatrix} e^{\lambda_{11}\, t} \cos\left(\frac{\pi}{10}x\right) + A_2 \begin{pmatrix}\alpha_{12}\\ \alpha_{22}\end{pmatrix} e^{\lambda_{12}\, t} \cos\left(\frac{2\pi}{10}x\right) \tag{59}$$

It is possible to plot the numerical solution for this case together with the analytical one given by equation (59), both normalised dividing by the maximum (of the order of $\mathrm{O}(e^{35})$):

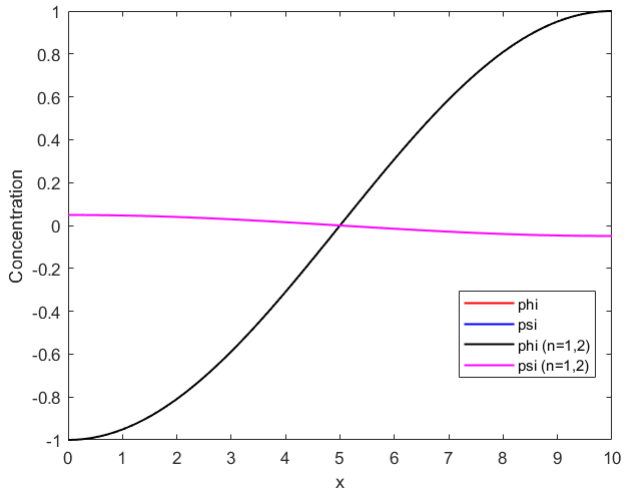

Figure 18: Concentrations normalised over space for system (54) with matrix (55), $t = 100$, $L = 10$, $D_\psi = 100$ and the general initial condition, with its corresponding curve where only $n = 1$ and $n = 2$ are taken into account, also normalised.

We can see that the curves apparently overlap for each concentration. Furthermore, if we consider the maximum error in both cases, we get that they are of the order of $\mathrm{O}(10^{-12})$ or even smaller, which is quite satisfactory. In addition, we can also see from Figure 18 that the dominating term of the solution is the one whose eigenvalue is higher, this is, $n = 1$, just as we anticipated before.

The solution has also an important dependence with the length L of the one-dimensional domain, since the number of n which have positive eigenvalues, depends strongly on this parameter, as we can see in equations (19) and (47), where $k_n = \frac{n\pi}{L}$. Moreover, as we have seen in the previous examples, the behaviour of the solution depends mainly on these particular values of n in the sense that more values of n with positive eigenvalues lead to a more complex solution, although in the end the solution will be dominated by the mode whose positive eigenvalue is higher. In the following table, we have studied those values of n which have a positive eigenvalue for different values of L and D_ψ to analyse its dependence (this is, the dependence of the solution) with respect to these two parameters.

D_ψ / L	1	5	10	15	20	25	100
10	-	-	1	$\{1,2\}$	$\{1,2,3\}$	$\{1,2,3,4\}$	$\{4,...,19\}$
100	-	1	$\{1,2\}$	$\{1,2,3\}$	$\{1,2,3,4\}$	$\{1,2,3,4,5\}$	$\{2,...,22\}$

Table 1: Values of n which have positive eigenvalues for different values of D_ψ and L for system (54) with matrix (55), keeping fixed $D_\phi = 1$.

At first sight, it seems that the number of n which have positive eigenvalues, this is, that contribute to the solution, increases with L and D_ψ. This behaviour can be particularly analysed by plotting these specific values of n versus L, which has been carried out in Figure 19.

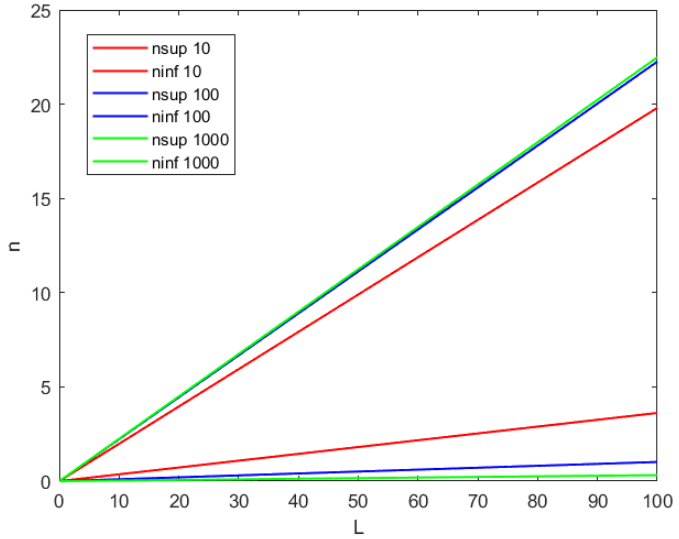

Figure 19: Values of n versus L for different values of D_ψ (10,100 and 1000), for system (54) with matrix (55). The ones that have positive eigenvalues are inside the region delimited by the lines of the same colour.

We can see in Figure 19 that both the upper and lower limits for n have a linear behaviour. From this plot, we can conclude that these values of n increase with L. This dependence is not particular of this case, but happens in general as we can expect from equation (47) where $k_n = \frac{n\pi}{L}$, being the bounds of k_n fixed by the other parameters. As a consequence, if L is increased, the interval of possible n is wider.

Moreover, this range of n also increases for higher values of D_ψ. This dependence can be seen in Figure 20 for a fixed value of L.

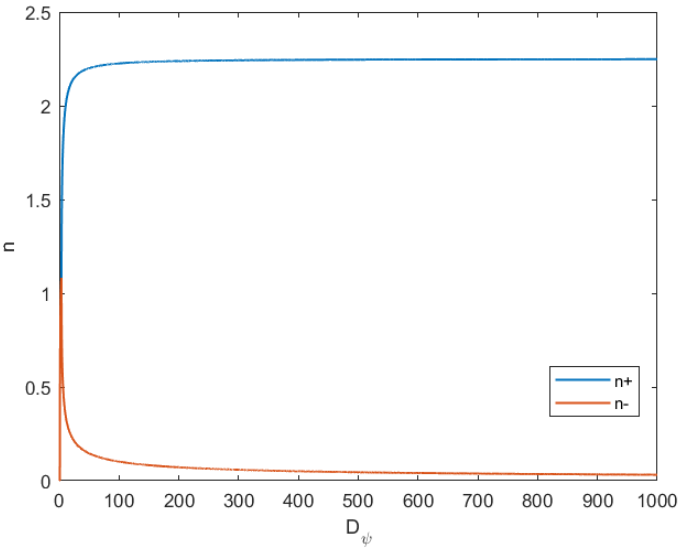

Figure 20: Values of n versus D_ψ for $L = 10$, for system (54) with matrix (55) . Those that have positive eigenvalues are inside the region delimited by both curves.

In this plot, we can see how the number of n with positive eigenvalues grows initially exponentially with D_ψ although this behaviour gets attenuated for approximately $D_\psi \approx 50$ to be stabilized asymptotically at $D_\psi \approx 100$. This means that, in this case, the variation is performed in the initial range of (0-50). In addition, from $D_\psi \approx 100$ onwards, no matter how much the value of D_ψ is increased, that the number of n which have positive eigenvalue will not change. This behaviour takes place in general for every value of L (as well as for other values of the other parameters), although it changes quantitatively being the variation higher for higher values of L. Furthermore, we have also seen that the concentrations increase earlier in time for higher values of L.

All in all, the complexity of the pattern depends mainly on the number of n that have positive eigenvalues which, as we have seen, has a direct correlation with the initial condition as well as with the values of L and the diffusivities.

We can also study a different matrix M, to see if simulations also match theoretical predictions.

$$M = \begin{pmatrix} 10 & -13 \\ 24 & -30 \end{pmatrix} \tag{60}$$

In this case, we will also consider $L = 10$, $D_\phi = 1$ and $D_\psi = 10$, for which the range of values of n that have positive eigenvalue is $\{2, 3, ..., 8\}$. The highest eigenvalue corresponds to $n = 5$, hence we expect it to dominate in the general case for time high enough.

Nevertheless, if we fix a value of n with the initial condition as it has been done previously, for instance with $(\phi(x,0), \psi(x,0)) = (3\cos\left(\frac{\pi}{L}x\right), -7\cos\left(\frac{\pi}{L}x\right))$, we observe an unexpected behaviour of the numerical solution. For smaller values of t (for instance, $t = 10$), only $n = 1$ performs in the solution as expected, as this is the unique mode fixed in the initial condition. However, if we let the system evolve until $t = 14$, we observe the following pattern:

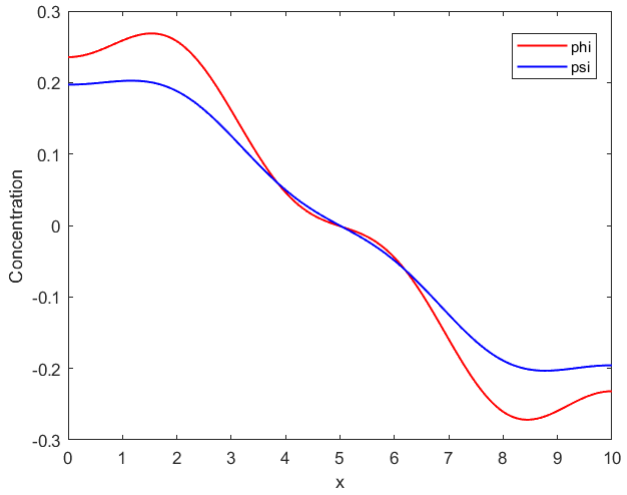

Figure 21: Concentrations over space for system (54) with matrix (60), where $L = 10$, $D_\psi = 10$, $t = 14$, and the initial condition is given by $(\phi(x,0), \psi(x,0)) = \left(3\cos\left(\frac{\pi}{L}x\right), -7\cos\left(\frac{\pi}{L}x\right)\right)$.

In Figure 21, there are unexpected contributions apart from $n = 1$, and its characteristic cosine form with only one node begins to be distorted. If we study a higher value of t, for instance, $t = 25$, we observe the following pattern, where now $n = 5$ is the dominant term:

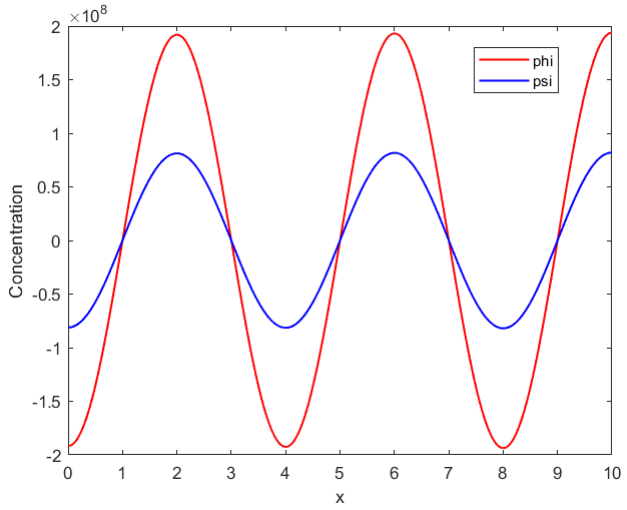

Figure 22: Concentrations over space for system (54) with matrix (60), where $L = 10$, $D_\psi = 10$, $t = 25$ and the initial condition is given by $(\phi(x,0), \psi(x,0)) = \left(3\cos\left(\frac{\pi}{L}x\right), -7\cos\left(\frac{\pi}{L}x\right)\right)$.

This does not agree with the analytical solution, according to which the solution tends to zero with time as $n = 1$ does not have a positive eigenvalue. Our interpretation is that this could be due to the computer arithmetic. Despite the initial condition includes only the term $\cos\left(\frac{\pi x}{10}\right)$, MATLAB might carry out the program considering an initial condition of the form $\cos\left(\frac{\pi x}{10}\right) + \mathrm{O}(\epsilon)\cos\left(\frac{5\pi x}{10}\right)$ where ϵ is of the order of $\mathrm{O}(10^{-16})$ (machine epsilon). Previous two initial conditions are numerically the same. However, if we let the system evolve in time, the positivity of the eigenvalue for $n = 5$ makes its contribution visible at a certain time, to end up being the main one for higher values of t.

Following this interpretation, it is possible to consider an analytic solution in which both terms $n = 1$ and $n = 5$ contribute. The coefficient accompanying the term corresponding to $n = 5$ is the ratio of the numerical solution to the exponential $e^{\lambda_{15}t}$ multiplied by the eigenvector of the analytical one, for a fixed time. This factor is of order $\mathrm{O}(10^{-14})$.

Therefore, we can now plot both numerical and the analytical solution normalised with the correction made. This is shown in Figure 23.

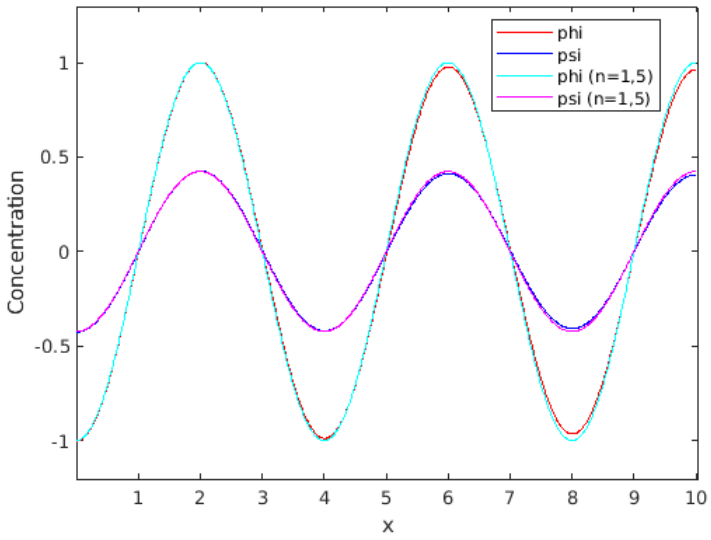

Figure 23: Concentrations over space for system (54) with matrix (60), where $L = 10$, $D_\psi = 10$, $t = 25$ and the initial condition is given by $(\phi(x,0), \psi(x,0)) = (3\cos\left(\frac{\pi}{L}x\right), -7\cos\left(\frac{\pi}{L}x\right))$. We have plotted it together with the interpretation given to the numerical difficulties found.

The overlap between both solutions in Figure 23 shows that both solutions are quite similar, hence we might be in the right track.

4.2.2 Non-Linear Problem

In this section, we will study the non-linear case for the one-dimensional problem:

$$\begin{cases} \begin{pmatrix} \phi_t(x,t) \\ \psi_t(x,t) \end{pmatrix} = \begin{pmatrix} f(\phi,\psi) \\ g(\phi,\psi) \end{pmatrix} + \begin{pmatrix} D_\phi & 0 \\ 0 & D_\psi \end{pmatrix} \begin{pmatrix} \phi_{xx}(x,t) \\ \psi_{xx}(x,t) \end{pmatrix} \\ \phi_x(0,t) = \phi_x(L,t) = 0, \quad \psi_x(0,t) = \psi_x(L,t) = 0 \\ \phi(x,0) = \phi_0(x), \qquad \psi(x,0) = \psi_0(x) \\ x \in \mathbb{D} = [0,L] \subset \mathbb{R}, \quad t > 0 \end{cases} \tag{61}$$

As it has been mentioned before, the linear theory has its limits, and this becomes evident in the following simulations, with the appearance of modes which are not expected to dominate, given the form of the initial condition. Another important difference, as we will see, are the concentration bounds. These differences with the linear case arise from the second order terms neglected in the linearization (12).

We are going to focus on the Schnakenberg system, where for instance, the non-linear terms are given in this case by

$$f(\phi,\psi) = 100 - 1000\,\phi + 1000\,\phi^2\psi \qquad g(\phi,\psi) = 900 - 1000\,\phi^2\psi$$

for which the constant solution is $(\phi_0, \psi_0) = (1,\ 0.9)$. Thus, the linearization matrix M is the following:

$$M = \begin{pmatrix} 800 & 1000 \\ -1800 & -1000 \end{pmatrix} \tag{62}$$

We can firstly study in this case the solution dependence with respect to L and D_ψ. This is shown in Table 3:

D_ψ / L	0.25	0.5	1	5	10
10	-	3	$\{5, 6, 7\}$	$\{23, ..., 35\}$	$\{46, ..., 71\}$
100	$\{1, 2\}$	$\{1, 2, 3, 4\}$	$\{2, ..., 8\}$	$\{6, ..., 44\}$	$\{12, ..., 88\}$

Table 2: Values of n which have positive eigenvalues for different values of D_ψ and L for system (61) with matrix (62), keeping $D_\phi = 1$ fixed.

We can see a similar dependence of these particular values of n with L and D_ψ, as in Table 1, in the sense that the range of values of n with positive eigenvalues increases with both parameters.

We can also analyse the behaviour of the solution with respect to the initial conditions, as we did in the linear case. For instance, we can choose $(\phi(x,0), \psi(x,0)) = \left(\phi_0 + cos\left(\frac{3\pi}{L}x\right), \psi_0 + cos\left(\frac{3\pi}{L}x\right)\right)$ for $L = 0.25$, $D_\phi = 1$ and $D_\psi = 10$, (i.e, there is no n with positive eigenvalue), and plot the solution against both space and time (Figures 24 and 25).

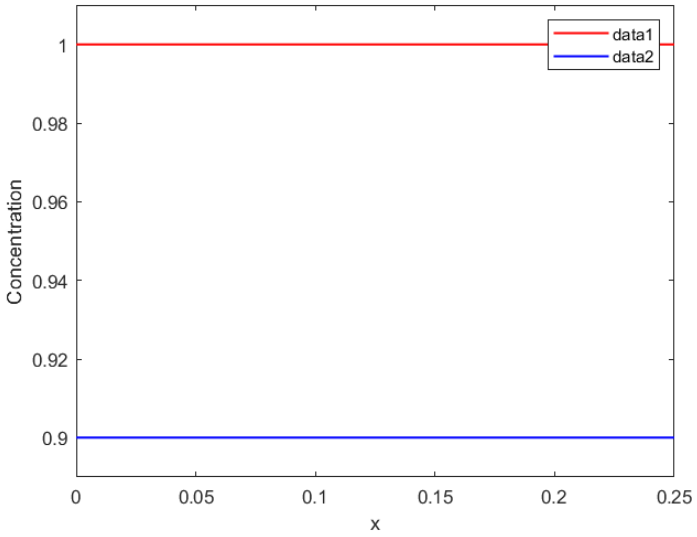

Figure 24: Concentrations over space for system (61) with matrix (62), $L = 0.25$, $D_\psi = 10$, $t = 10$ and the initial condition explained before.

We can see in Figure 24 that there is no spatial pattern. This is what we expected since the constant solution is only perturbated with $n = 3$ and, as stated above, none of the values of n have positive eigenvalue. Moreover, since the constant solution is asymptotically stable, the perturbated concentrations quickly tend to it, as it can be seen in Figure 25.

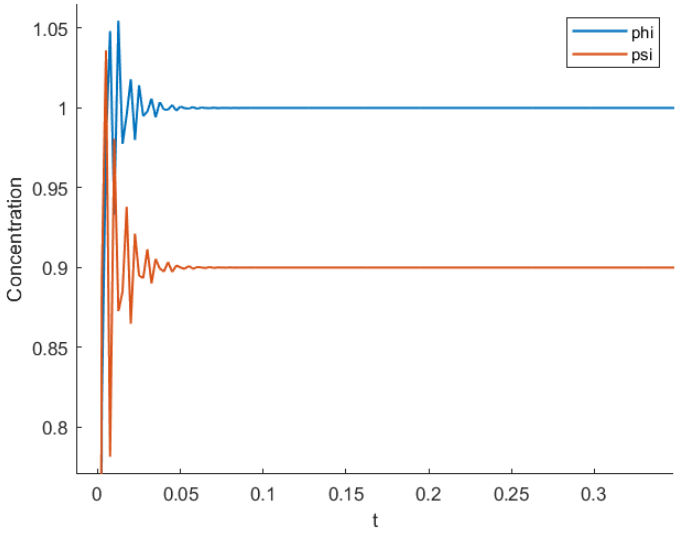

Figure 25: Concentrations over time for system (61) with matrix (62), $L = 0.25$, $D_\psi = 10$, $t = 10$ and the initial condition explained before.

If we consider $L = 0.5$ with the same initial condition, we would see that the main contribution corresponds to $n = 3$ since it is the only value of n with a positive eigenvalue for this particular L apart from the fact that we have fixed this value in the initial condition. This is the same as in the linear case, so we do not show the results in order to not to be repetitive.

However, for $L = 1$ and the same initial condition, we have a different result from the linear case, where the main contribution was $n = 3$ (fixed in the initial condition). The solution for the non-linear case is shown in Figure (26):

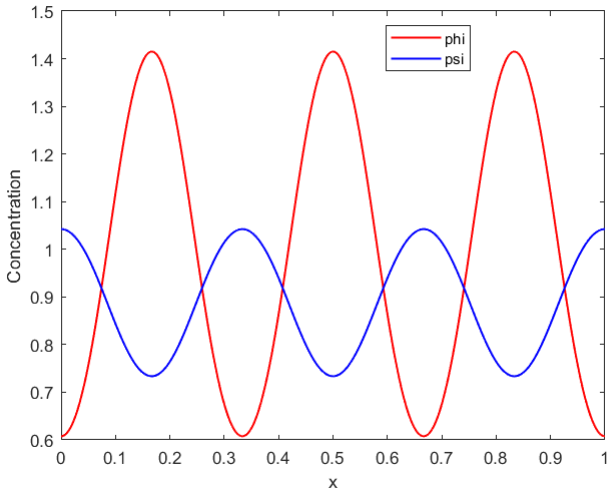

Figure 26: Concentrations over space for system (61) with matrix (62), $L = 1$, $D_\psi = 10$, $t = 10$ and the initial condition $(\phi(x,0), \psi(x,0)) = \left(\phi_0 + cos\left(\frac{3\pi}{L}x\right), \psi_0 + cos\left(\frac{3\pi}{L}x\right)\right)$.

We can see that the main contribution to the solution in Figure 26 is the term corresponding to $n = 6$ as there are six nodes. Despite fixing $n = 3$ in the initial condition, it is $n = 6$ the one that dominates. This, as it has been explained before, arises from the neglection of the second order terms in the linearisation of the problem. Although these terms are small, the highest positive eigenvalue corresponds to $n = 6$, hence it dominates for sufficiently high values of t.

It is possible to study also a general initial condition as in the linear case, where $(\phi(x, 0), \psi(x, 0)) = (x^2, x^3)$, for $L = 1$:

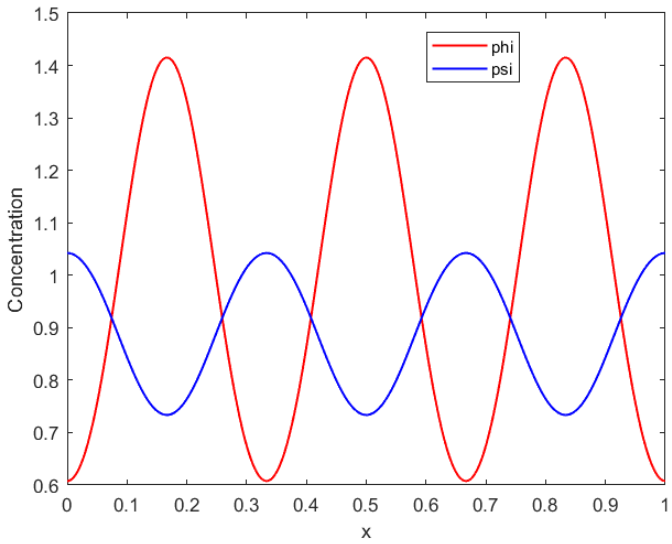

Figure 27: Concentrations over space for system (61) with matrix (62), $L = 1$, $D_\psi = 10$, $t = 10$ and the general initial condition explained before.

Again, we can observe in Figure 27 that the dominant term is $n = 6$. This behaviour matches with predictions made by linear theory, as no mode is fixed in the initial conditions. Note that Figures 26 and 27 are identical even though the initial conditions were completely different, hence the importance of the non-linear terms stands out.

From the results obtained for the non-linear case, we can conclude that the differences with respect to the linear one are quite evident. Note in the last case the presence of unexpected modes and the fact that concentrations are positive and bounded. Thus, although linear theory provides insight into what one might expect in the non-linear case, its applicability is limited. This will become more evident in the two and three spatial dimensions simulations.

4.3. Spatial dimension two

4.3.1 Linear Problem

This is a more complex problem where we have an additional dimension. In this case, we are going to study the normalised Schnakenberg problem, starting with the analysis of the linearized problem:

$$\begin{cases} \begin{pmatrix} \phi_t(x,t) \\ \psi_t(x,t) \end{pmatrix} = M \begin{pmatrix} \phi(x,t) \\ \psi(x,t) \end{pmatrix} + \begin{pmatrix} 1 & 0 \\ 0 & d \end{pmatrix} \begin{pmatrix} \Delta\phi(x,t) \\ \Delta\psi(x,t) \end{pmatrix} \\ \nabla\phi(x,t)\cdot\vec{n} = 0, \quad \nabla\psi(x,t)\cdot\vec{n} = 0, \quad x \in \partial\mathbb{D} \\ \phi(x,0) = \phi_0(x), \qquad \psi(x,0) = \psi_0(x) \\ x \in \mathbb{D} = [0, L_x] \times [0, L_y] \subset \mathbb{R}^2, \;\; t > 0 \end{cases} \tag{63}$$

where the matrix M is given by

$$M = \gamma \begin{pmatrix} \frac{b-a}{a+b} & (a+b)^2 \\ \frac{-2b}{a+b} & -(a+b)^2 \end{pmatrix} \tag{64}$$

We have initially chosen $L_x = L_y = 1$, $a = 0.126779$, $b = 0.792366$, $d = 10$ and $\gamma = 60$ as Turing conditions are fulfilled with these parameters, with only a pair of values of n_x and n_y for which we have a positive eigenvalue : $\{n_x, n_y\} = \{1, 1\}$, being $\lambda_{11_+} = 2.8084$.

As we did in the one dimensional problem, we begin with a simple case in which the modes performing in the solution do not have positive eigenvalue. For instance,$(\phi(x,0), \psi(x,0)) = \left(a + b + \cos(2\pi\, x)\, \cos(\pi\, y)\,, \frac{b}{(a+b)^2} + \cos(2\pi\, x)\, \cos(\pi\, y)\right)$, hence fixing the pair $\{n_x, n_y\} = \{2, 1\}$. This is shown in Figure 28.

From this plot, we can visualize there is no pattern (as expected), since the only mode fixed in the initial condition (hence performing in the solution) has negative eigenvalues.

Eventually, it could be useful to study a more general case, for instance, given by the initial condition $(\phi(x,0), \psi(x,0)) = \left(a + b + x^2y^3, \frac{b}{(a+b)^2} + x^2y^3\right)$, where no pair of $\{n_x, n_y\}$ is fixed. The corresponding solution is shown in Figure 29:

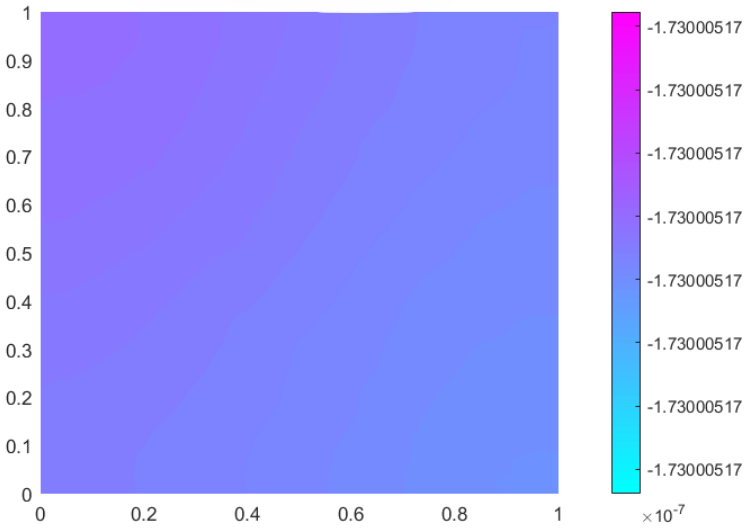

Figure 28: Two-dimensional pattern for the linearized problem of Schnakenberg (63) with matrix (64), $L_x = 1$, $L_y = 1$, $a = 0.126779$, $b = 0.792366$, $d = 10$, $\gamma = 60$, $t = 4$ and the initial condition mentioned before. The colour represents ϕ concentration.

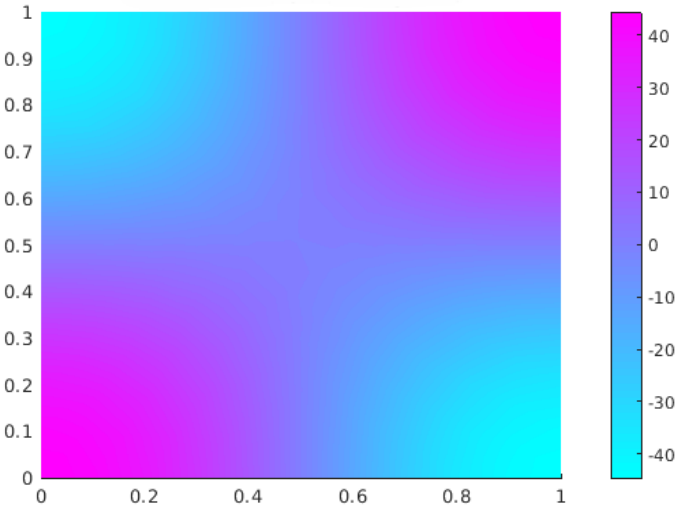

Figure 29: Two-dimensional pattern for the linearized problem of Schnakenberg (63) with matrix (64), with $L_x = 1$, $L_y = 1$, $a = 0.126779$, $b = 0.792366$, $d = 10$, $\gamma = 60$, $t = 2$ and the initial condition mentioned before. The colour represents ϕ concentration.

In this case, we have a pattern where the dominant mode is the pair $\{n_x, n_y\} = \{1, 1\}$, the only one which has positive eigenvalue. This was what we expected from linear theory. In addition, if we let the system evolve indefinitely, the concentration increases unboundedly. For instance, for $t = 4$ we already have a concentration of the order of $O(10^4)$.

Revisiting section 3.2, γ and d become especially important in pattern formation and, as one might expect extrapolating the analysis of the one-dimensional problem, if we increase γ and d, there will exist more $\{n_x, n_y\}$ pairs performing in the solution. We analyse this correlation in Table 3.

d / γ	20	30	60	100
10	-	$\{1,0\}$	$\{1,1\}$	$\{2,0\},\{1,1\}$
20	$\{1,0\}$	$\{1,0\}$	$\{1,0\},\{1,1\}$	$\{1,0\},\{1,1\},\{2,0\},\{2,1\}$

d / γ	200
10	$\{2,0\},\{2,1\},\{2,2\},\{3,0\}$
20	$\{1,1\},\{2,0\},\{2,1\},\{2,2\},\{3,0\},\{3,1\}$

Table 3: Values of n which have positive eigenvalues for different values of d and L for the linearized problem of Schnakenberg (63) with matrix (64), $L_x = 1$, $L_y = 1$, $a = 0.126779$, $b = 0.792366$. For simplicity, the pair $\{n_x, n_y\}$ represents both $\{n_x, n_y\}, \{n_y, n_x\}$

.

We can also study a more complex problem with the same general initial condition as in the previous case. This is achieved by increasing both γ and d, as there are more modes performing. For instance, considering $\gamma = 1000$ and $d = 20$, we get the following pattern:

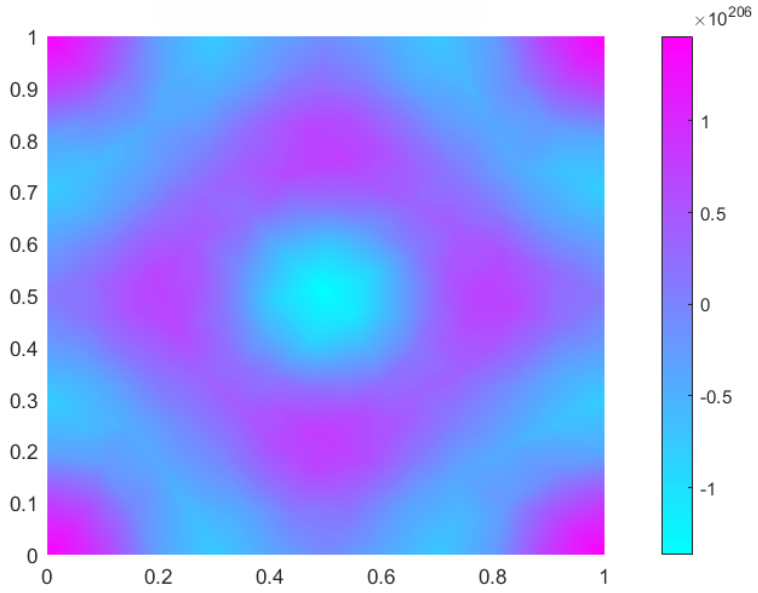

Figure 30: Two-dimensional pattern for the linearized problem of Schnakenberg (63) with matrix (64), $L_x = 1$, $L_y = 1$, $a = 0.126779$, $b = 0.792366$, $d = 20$, $\gamma = 1000$, $t = 2$ and the general initial condition mentioned before. The colour represents ϕ concentration.

Although the dominant eigenvalue corresponds to the pairs $\{2,4\}$ and $\{4,2\}$, it is more difficult to appreciate its contribution; partly due to the variety of modes performing in the solution, as there are 48 of them. However, it is important to be aware of the distorsion arising from the fact that both dominant pairs have the same eigenvalue, hence contribute in the same way. Since this eigenvalue $\lambda_{42_+} = 2.3715e+02$ is considerably high, the concentrations increase very quickly, being already of the order of $\mathrm{O}(10^{206})$ for $t = 2$.

4.3.2 Non-Linear Problem

We will carry out the same analysis as in the linear problem, to compare the differences between both problems. The system in this case is given by:

$$\begin{cases} \begin{pmatrix} \phi_t(x,t) \\ \psi_t(x,t) \end{pmatrix} = \begin{pmatrix} \gamma\left(a - \phi + \phi^2\psi\right) \\ \gamma\left(b - \phi^2\psi\right) \end{pmatrix} + \begin{pmatrix} 1 & 0 \\ 0 & d \end{pmatrix} \begin{pmatrix} \Delta\phi(x,t) \\ \Delta\psi(x,t) \end{pmatrix} \\ \nabla\phi(x,t)\cdot\vec{n} = 0, \quad \nabla\psi(x,t)\cdot\vec{n} = 0, \quad x \in \partial\mathbb{D} \\ \phi(x,0) = \phi_0(x), \qquad \psi(x,0) = \psi_0(x) \\ x \in \mathbb{D} = [0, L_x] \times [0, L_y] \subset \mathbb{R}^2, \;\; t > 0 \end{cases} \tag{65}$$

Considering the same parameters and starting with the constant initial condition $(\phi_0, \psi_0) = \left(a+b, \frac{b}{(a+b)^2}\right)$, we get the following pattern for $t = 2$:

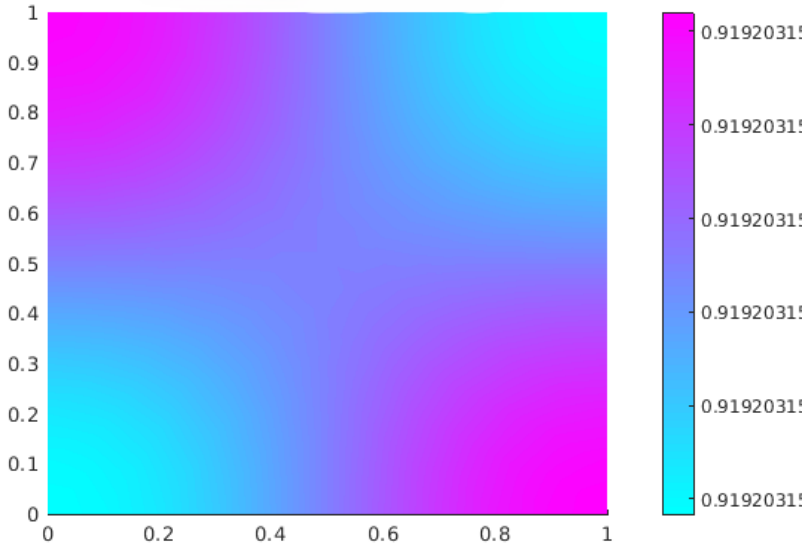

Figure 31: Two-dimensional pattern for the Schnakenberg system (65), with $L_x = 1$, $L_y = 1$, $a = 0.126779$, $b = 0.792366$, $d = 10$, $\gamma = 60$, $t = 2$ and the constant initial conditions mentioned before. The colour represents ϕ concentration.

Whereas in the linear system for this case concentrations would tend to zero (as this is the constant solution in the linear case), we now see they remain the same over time. Despite the initial condition is the same in both cases, (ϕ_0, ψ_0) is the stationary constant solution for the non-linear case, which is asymptotically stable, hence we do not have pattern and concentrations tend to this stationary solution.

Let us consider

$$(\phi(x,0), \psi(x,0)) = \left(a + b + \cos(2\pi\, x)\, \cos(\pi\, y)\,, \frac{b}{(a+b)^2} + \cos(2\pi\, x)\, \cos(\pi\, y)\right):$$

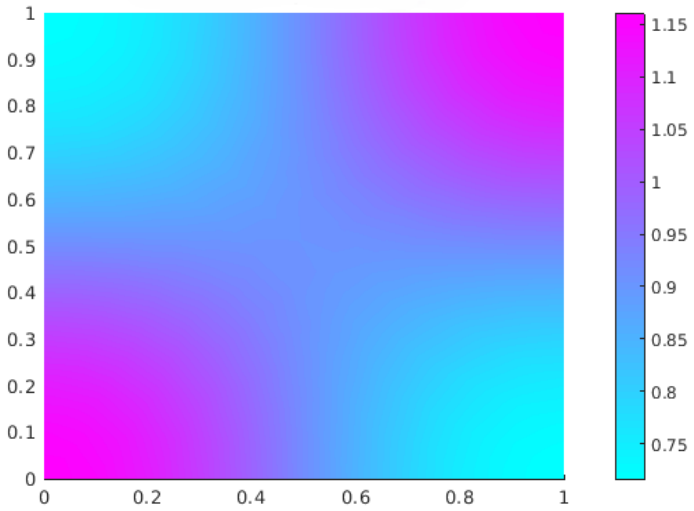

Figure 32: Two-dimensional pattern for the Schnakenberg system (65), with $L_x = 1$, $L_y = 1$, $a = 0.126779$, $b = 0.792366$, $d = 10$, $\gamma = 60$, $t = 2$ and the initial condition mentioned before. The colour represents ϕ concentration.

In this case, although the only pair performing in the initial condition is $\{n_x, n_y\} = \{2, 1\}$, the dominant mode in Figure 32 corresponds to $\{n_x, n_y\} = \{1, 1\}$, which arises from the non-linear terms. In addition we can also appreciate the effect of the non-linear terms interaction, bounding the concentrations, in contrast with the linear case where the concentrations were of the order of $\mathrm{O}(10^4)$ for $t = 4$.

As far as for the general case is concerned, we show the corresponding pattern in Figure 33, also bounded by the non-linear terms, where, as in previous cases, the contribution of the dominant mode is remarkable.

Eventually we can study the last example analysed in Figure 30, for the non-linear case. This has been carried out in Figure 34.

With this last example, the limitations of the linear theory become obvious. Whereas in the Figure 30, the pattern obtained is blurry, and the algorithm suffers as a consequence of the quickly and unbounded growth of the concentration, in Figure 34, the concentrations are bounded by the non-linear terms interaction, hence the algorithm works more efficiently. Despite having a wide range of modes with positive eigenvalue, it is possible to distinguish the dominant modes $\{2, 4\}, \{4, 2\}$ from those whose eigenvalue is smaller.

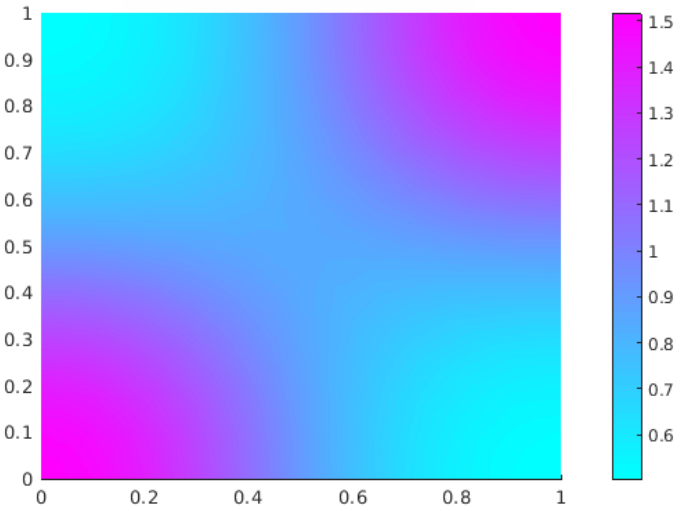

Figure 33: Two-dimensional pattern for the Schnakenberg system (65), with $L_x = 1$, $L_y = 1$, $a = 0.126779$, $b = 0.792366$, $d = 10$, $\gamma = 60$, $t = 2$ and the general initial condition mentioned before. The colour represents ϕ concentration.

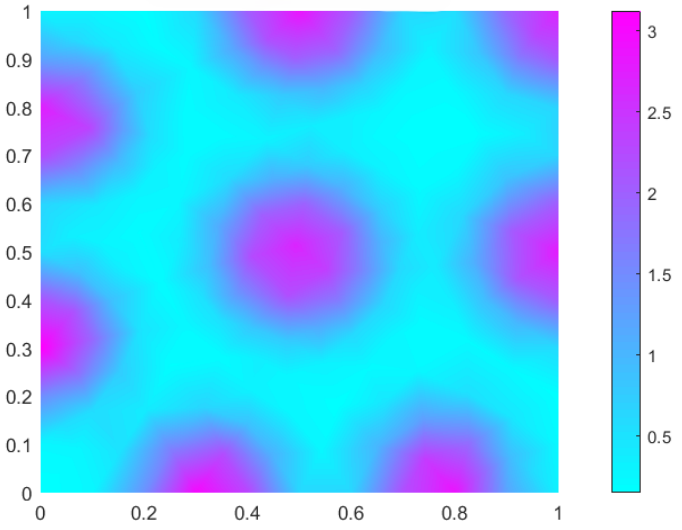

Figure 34: Two-dimensional pattern for the Schnakenberg system (65), with $L_x = 1$, $L_y = 1$, $a = 0.126779$, $b = 0.792366$, $d = 20$, $\gamma = 1000$, $t = 2$ and the general initial condition $(\phi(x,0), \psi(x,0)) = \left(a + b + x^2y^3, \frac{b}{(a+b)^2} + x^2y^3\right)$. The colour represents ϕ concentration.

4.4. Spatial dimension three

4.4.1 Linear Problem

Finally, we can carry out the same analysis for the three-dimensional problem. We will also consider the linearized version of Schnakenberg system

$$\begin{cases} \begin{pmatrix} \phi_t(x,t) \\ \psi_t(x,t) \end{pmatrix} = M \begin{pmatrix} \phi(x,t) \\ \psi(x,t) \end{pmatrix} + \begin{pmatrix} 1 & 0 \\ 0 & d \end{pmatrix} \begin{pmatrix} \Delta\phi(x,t) \\ \Delta\psi(x,t) \end{pmatrix} \\ \nabla\phi(x,t)\cdot\vec{n} = 0, \quad \nabla\psi(x,t)\cdot\vec{n} = 0, \quad x \in \partial\mathbb{D} \\ \phi(x,0) = \phi_0(x), \qquad \psi(x,0) = \psi_0(x) \\ x \in \mathbb{D} = [0,L_x]\times[0,L_y]\times[0,L_z] \subset \mathbb{R}^3, \ \ t > 0 \end{cases} \tag{66}$$

where the matrix M is given by:

$$M = \gamma \begin{pmatrix} \frac{b-a}{a+b} & (a+b)^2 \\ \frac{-2b}{a+b} & -(a+b)^2 \end{pmatrix}$$

Although in general linear theory is expected to be more easy to deal with than the non-linear case, the fact that its solutions grow exponentially, entails numerical difficulties which increase in three spatial dimensions. Therefore, we have chosen the parameters so that these difficulties are overcome since we already know that high values of γ and d involves more complex patterns. With this aim, we have considered $L_x = 1, L_y = 1, L_z = 1, a = 0.25, b = 0.75, d = 25$, $\gamma = 100$ and an initial condition given by $(\phi(x,0),\psi(x,0)) = (\phi_0 + 10^{-3}\sin\pi x, \psi_0 + 10^{-4}\sin\pi x)$. We have 4 modes with positive eigenvalues, where $\{1,1,0\},\{0,1,1\}$ and $\{1,0,1\}$ are the dominant ones. The pattern obtained is shown in Figure 35:

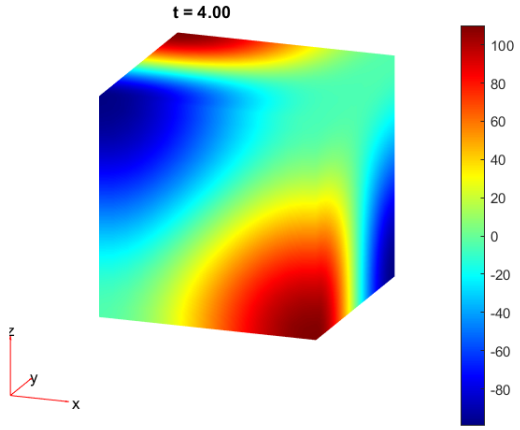

Figure 35: Three-dimensional pattern for the Schnakenberg system, where $L_x = 1$, $L_y = 1$, $L_z = 1$ $a = 0.25, b = 0.75, d = 25$, $\gamma = 100$, $t = 4$ and the general initial condition $(\phi(x,0),\psi(x,0)) = \left(\phi_0 + 10^{-3}\sin(\pi x), \psi_0 + 10^{-4}\cos(\pi x)\right)$.

Despite the dominant modes are predicted by linear theory, it is more difficult to distinguish them clearly. This already happened in the two dimensional case, where the pattern arises from the joint contribution of the dominant modes, hence we are visualizing the superposition of all of them.

In Figure 36 it is possible to observe the pattern inside the volume by drawing the corresponding contours slice planes.

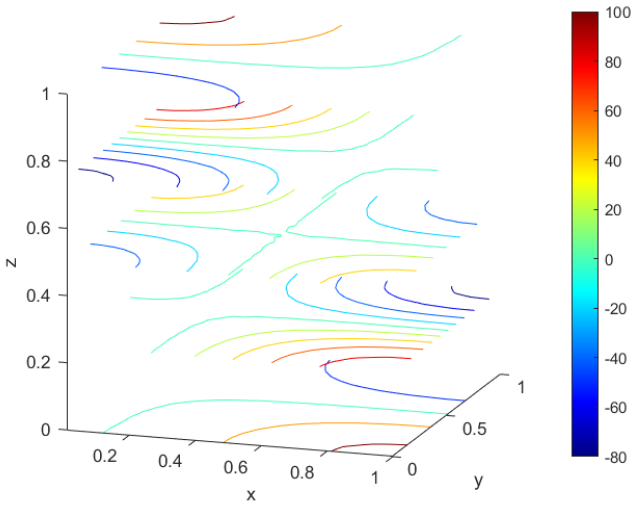

Figure 36: Five contours in volume slice planes of Figure 35

We can observe how concentrations tend to decay smoothly if we move away from the locations with highest concentrations. This can be seen more clearly if we plot only the contour slice corresponding to $z = 0.5$, where we can see that the highest values in modulus for the concentrations are located in the corners.

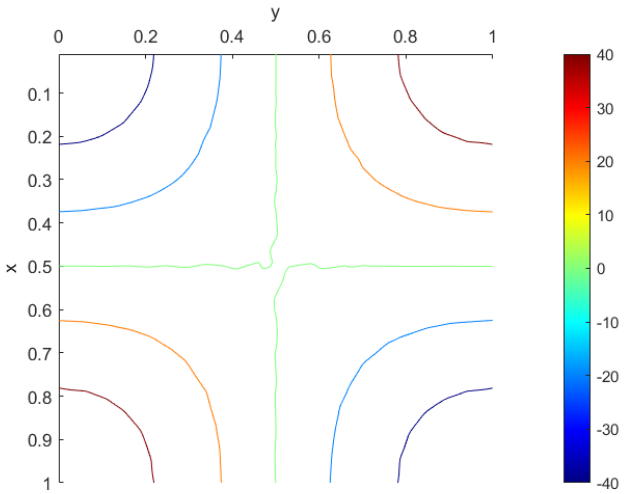

Figure 37: Contuor slice of $z = 0.5$ for Figure 35.

4.4.2 Non-Linear Problem

The problem to be adressed in this case is the three-dimensional Schnakenberg system:

$$\begin{cases} \begin{pmatrix} \phi_t(x,t) \\ \psi_t(x,t) \end{pmatrix} = \begin{pmatrix} \gamma\left(a - \phi + \phi^2\psi\right) \\ \gamma\left(b - \phi^2\psi\right) \end{pmatrix} + \begin{pmatrix} 1 & 0 \\ 0 & d \end{pmatrix} \begin{pmatrix} \Delta\phi(x,t) \\ \Delta\psi(x,t) \end{pmatrix} \\ \nabla\phi(x,t)\cdot\vec{n} = 0, \quad \nabla\psi(x,t)\cdot\vec{n} = 0, \quad x \in \partial\mathbb{D} \\ \phi(x,0) = \phi_0(x), \qquad \psi(x,0) = \psi_0(x) \\ x \in \mathbb{D} = [0, L_x] \times [0, L_y] \times [0, L_z] \subset \mathbb{R}^3, \quad t > 0 \end{cases} \tag{67}$$

We have studied the case given by $a = 0.2, b = 0.8, d = 25$ and $\gamma = 100$. As for the initial condition is concerned, we have considered a simple one: $(\phi(x,0 =, \psi(x,0)) = (\phi_0 + 10^{-2}\sin(\pi\, x), \psi_0 + 10^{-3}\cos(\pi\, x))$

In this case, we have 10 modes with positive eigenvalue, among which $\{1,1,0\}, \{0,1,1\}$ and $\{1,0,1\}$ have the highest ones. The pattern obtained in this case is shown in Figure 38:

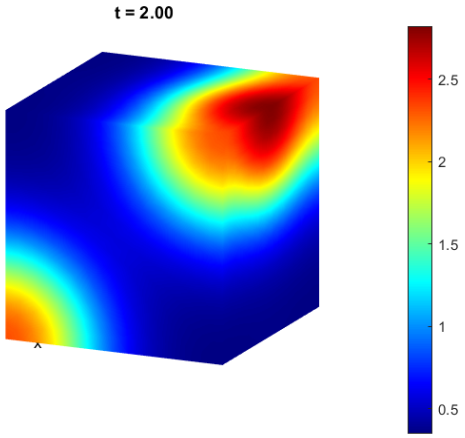

Figure 38: Three-dimensional pattern for the Schnakenberg system (67) with $L_x = 1$, $L_y = 1$, $L_z = 1$ $a = 0.2$, $b = 0.8$, $d = 25$, $\gamma = 100$, $t = 2$ and the general initial condition $(\phi(x,0 =, \psi(x,0)) = \left(\phi_0 + 10^{-2}\sin(\pi\, x), \psi_0 + 10^{-3}\cos(\pi\, x)\right)$.

From Figure 38, we can see that concentrations are positive, being the highest values located along two cube edges. Concentrations are bounded and they do not change too much from $t = 2$ onwards. Moreover, we can analyse the pattern further, through the contour slices.

Figure 39 enhances what we mentioned previously, as we can visualize how the concentration tends to decay as we move away from those edges.

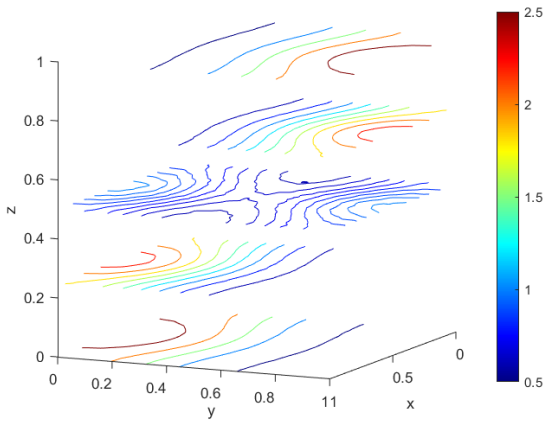

Figure 39: Five contour slices from the cube volume

Eventually, we can also try to carry out the simulations in more complex domains. For instance, once at this point, the study of pattern formation in animals is is worthy of attention. As an example, we have used an stl file of a polygonal cat with 13 faces in order to carry out a simulation.

With this aim, we show in Figure 40 the results obtained for a cat, with $\gamma = 1, d = 55, a = 0.22, b = 0.58$ and a general condition given by $(\phi(x,0), \psi(x,0)) = (\phi_0 + 0.8\cos(\pi x)\cos(\pi y)\cos(\pi z), \psi_0 + 0.8\cos(\pi x)\cos(\pi y)\cos(\pi z))$:

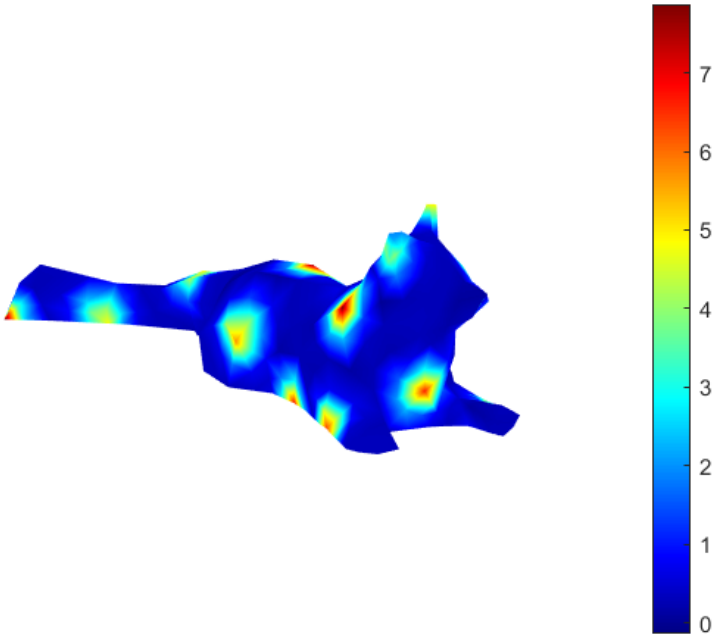

Figure 40: Three-dimensional pattern, considering Schnakenberg model solved when $\mathbb{D}$ is the figure of a cat, with $\gamma = 2, d = 55, a = 0.22, b = 0.58, t = 10$ and the general initial condition

5. Conclusions

In this work, we have studied Turing's theory of morphogenesis. In 1952, he proposed a two nonlinear reaction-diffusion partial differential equations to explain the formation of spatial biological patterns. We have firstly used linear theory to obtain both the exact solutions of the linearized problem, and the general conditions that these types of systems must satisfy for such patterns to emerge. Afterwards, we have exploited the formulas obtained in the linear case to the non-linear problem, and we have become aware of the advantages and limitations of linear theory.

We have been able to predict to a good extent the behaviour of the solutions, determining the range of modes performing in the solution and so on. However, we have encountered several differences in the solutions for the linear case, which have complicated the analysis in the non-linear problem. Whereas in the former the solutions can be negative and grow exponentially and unboundedly, in the latter they are positive and bounded when the initial data are also. Nevertheless, we have not found any proof of this behaviour in the literature for the Schnakenberg model. In this context, numerical simulations performed with MATLAB have shown to be crucial in understanding the dynamics of the reaction-diffusion systems. We conducted simulations for one, two, and three spatial dimensions, which significantly enhanced our comprehension of the pattern formation processes, understanding the dependencies of the solution with respect to the different parameters involved in the system. In particular, we have seen the relations required for the Schnakenberg model, for a and b so that Turing conditions are satisfied as well as understood the tuning role γ and d play as for the range of modes is concerned. This system was studied for a variety of geometry configurations where the last example should be remarked. In this case, we wanted to study a more complex domain, for which is was necessary to use another tool outside of MATLAB, which is an STL file.

During the simulations, we faced significant challenges, especially with the linear case, where the algorithms suffered given the exponential growth of the data. Moreover, we also encountered unexpected behaviour of the solutions in a particular case, for which we carried out our own interpretation.

References

[1] C.H.L. Beentjes. *Pattern Formation Analysis in the Schnakenberg Model*. Technical Report, Mathematical Institute, University of Oxford, Oxford, UK, 2015.

[2] L.A. Fernández. *Introducción a las Ecuaciones en Derivadas Parciales*, 2022. Departamento de Matemáticas, Estadística y Computación, Universidad de Cantabria.

[3] D. Jou. La influencia de Turing en la biología. *Mètode*, 2012.

[4] A. Krause. A modern view on Turing's theory of pattern formation. The Royal Society, 2021. Accessed on: 2024-05-19.

[5] J.D. Murray. *Mathematical Biology: I. An Introduction*. Springer, 2001.

[6] J.D. Murray. *Mathematical Biology: II Spatial Models and Biomedical Applications*. Springer, 2003.

[7] J. Raspopovic et al. Digit patterning is controlled by a Bmp-Sox9-Wnt Turing network modulated by morphogen gradients. *Science*, Vol 345:566–570, 2014. https://www.science.org/doi/10.1126/science.1252960.

[8] F. Rothe. *Global Solutions of Reaction-Diffusion Systems*. Springer, Berlin, Heidelberg, 1984.

[9] P. K. Maini T. E. Woolley, R. E. Baker. Turing's theory of morphogenesis: Where we started, where we are and where we want to go. *The Incomputable*, page 219–235, 2017. https://doi.org/10.1007/978-3-319-43669-2_13.

[10] E. Schrödinger. *What is life? Mind and matter*. Cambridge University Press, 1967.

[11] D. W. Thompson. *On growth and form*. University press, 1917.

[12] A.M. Turing. The chemical basis of morphogenesis. *Philosophical Transactions of the Royal Society of London*, 237(641):37–72, 1952. https://doi.org/10.1098/rstb.1952.0012.

[13] C.H. Waddingtong. Organisers and genes. *The American Midland Naturalist*, 30(3):811–812, 1943. https://doi.org/10.2307/2421224.

A. Appendix: MATLAB programs

A.1. Pdepe program

```
%% Global parameters
global L D1 D2 T A
T=100;
L=10;
nx=100*L;
nt=100*T;
D1=1; D2=100;
x=linspace(0,L,nx);
t=linspace(0,T,nt);
m=0;
A=[1/2 1;-0.55 -1];
opciones=odeset('RelTol',1e-6);
sol = pdepe(m,@pdefun,@pdeic,@pdebc,x,t,opciones);
%--------------------------------------------------------------------------
function [c,D,s] = pdefun(x,t,u,dudx)    %PDE system
global D1 D2 A
c = [1; 1];
D = [D1; D2] .* dudx;
f=A(1,1)*u(1)+A(1,2)*u(2);
g=A(2,1)*u(1)+A(2,2)*u(2);
s = [f; g];
end
%--------------------------------------------------------------------------
function u0 = pdeic(x) %Initial condition
global L
% phi0=3*cos(pi*x/L);
% psi0=-7*cos(pi*x/L);
phi0=x.^2;
psi0=x.^3;
u0=[phi0;psi0];
end
%--------------------------------------------------------------------------
function [pl,ql,pr,qr] = pdebc(xl,ul,xr,ur,t) % Boundary Conditions
pl = [0; 0];
ql = [1; 1]; %Neumann left condition
pr = [0; 0];
qr = [1; 1]; %Neumann right condition
end
%--------------------------------------------------------------------------
```

A.2. Solvepde program for spatial dimension three

```
%% Global Parameters
global Lx Ly Lz D1 D2 a b gamma
gamma=800;
Lx=1;
Ly=1;
Lz=1;
a=0.2000;
b=0.3842;
D1=1; D2=20;
A=gamma*[(b-a)/(a+b), (a+b)^2; (-2*b)/(a+b),  -(a+b)^2];
%%%%%%%%%%%%%%%%%%%%%%%%%%%%%%%%%%%%%%%%%%%%%%%%%%%%%%%%%%%%%%%%%%%%%%%%%%%%%%%
% Create a two equations PDE model
model = createpde(2);
importGeometry(model, 'Cubo1.stl');
mesh = generateMesh(model, "GeometricOrder", "linear");

% Adjust the transparency of the cube's faces
figure;
pdegplot(model, 'FaceAlpha', 0.3, 'FaceLabels', 'on');
title('Cubo con Caras Transparentes');

% Parameters of the system
d = 1;
c = [D1;D2];
f = @(region,state) [gamma*(a - state.u(1,:) + state.u(1,:).^2 .*
 ↪  state.u(2,:));
                     gamma*(b - state.u(1,:).^2 .* state.u(2,:))];

%Boundary Conditions
applyBoundaryCondition(model, 'face', (1:6), 'g', 0, 'q', 0);

specifyCoefficients(model, 'm', 0, 'd', d, 'c', c, 'a', 0, 'f', f);

% Initial condition
u0 = @(region) [(a+b)*ones(size(region.x)) +
 ↪  (region.x).*(region.y).*(region.z);...
    b/(a+b)^2*ones(size(region.x))+(region.x).*(region.y).*(region.z)];
setInitialConditions(model, u0);

%Time vector and resolution of the system
tlist = linspace(0,2,10);
result = solvepde(model, tlist);
u = result.NodalSolution;

figure;
    pdeplot3D(model, 'ColorMapData', u(:,1,end));
```

```
45      alpha(0.5);
46      title(sprintf('Solución en t = %.2f', tlist(end)));
47      drawnow;
48
49  %Contour slices of the volume
50  component = 1;
51  xx = -0.5:0.01:0.5;
52  yy = -0.5:0.01:0.5;
53  zz = 0:0.01:1;
54  [X, Y, Z] = meshgrid(xx, yy, zz);
55
56  % Interpolate the solution for the first component at all times
57  uintrp = interpolateSolution(result, X, Y, Z, component,length(tlist));
58
59  % We redefine the size of the vector
60  sizeX = size(X);
61   uintrp = reshape(uintrp, size(X));
62
63  % Visualize the solution with countourslice of several values of z
64  figure
65  colormap jet
66
67  altura = [0; 1/6; 2/6;3/6;4/6;5/6;1];
68  contourslice(X, Y, Z, uintrp, [], [], altura)
69  xlabel('x')
70  ylabel('y')
71  zlabel('z')
72  colorbar
73  view(-11, 14)
74  axis equal
```